UNITED STATES DEPARTMENT OF THE INTERIOR

GEOLOGICAL SURVEY

An analysis of thermal data from the vicinity of Cajon Pass, California

by

J. H. Sass[1], A. H. Lachenbruch[2], S. P. Galanis, Jr.[2], R. J. Munroe[2], and T. H. Moses, Jr.[2]

Open File Report 86-468

[1]U.S. Geological Survey, Flagstaff, AZ 86001
[2]U.S. Geological Survey, Menlo Park, CA 94025

1986

Abstract

Twenty-two heat-flow determinations and eight estimates (from thermal gradients) in the region near Cajon Pass indicate a somewhat more complex thermal regime than was heretofore apparent. At the Cajon Pass site, a combination of Pleistocene-Holocene uplift and erosion, topography, and a steeply dipping but poorly characterized contact between rocks of differing thermal conductivity introduce large uncertainties into the value for regional heat flow to 1.8 km. Heat flow near the San Andreas fault and within the Mojave Block averages about 70 mWm^{-2} but may be underestimated by 10% or so owing to systematic effects of climatic changes and downward water flow in the upper 150 to 200 meters.

INTRODUCTION

The first DOSECC-sponsored continental scientific drill hole is planned for a site near Cajon Pass north of San Bernardino, California (Figure 1). The primary scientific goal of this well is to provide data bearing on the fact that there is no observational evidence for a heat-flow anomaly over the San Andreas fault in spite of experimental evidence for high friction, a paradox (Henyey, 1968; Brune and others, 1969; Henyey and Wasserburg, 1971; Lachenbruch and Sass, 1973, 1980). Interpretation of the heat flow from the existing 1.8 km well at this site is complicated by the structure and Pleistocene - Holocene tectonic history of the Transverse Ranges (Lachenbruch and others, 1986a, b).

As background information for thermal studies related to the Cajon Pass project, we here present information on temperatures, thermal conductivities, heat flow and heat production for the existing Cajon Pass well and for a number of other wells in the western Mojave Desert and adjacent Transverse Ranges.

HEAT FLOWS

For completeness sake, heat flows previously published by Henyey and Wasserburg (1971) are also presented in Table 1. The overall quality of the latter data is comparable to that of our own, except that Henyey and Wasserburg (1971) typically measured many more thermal conductivities for a given well than we did. Our choice of fewer samples per well was dictated by a number of practical considerations. In addition, we are satisfied that the average of 5 to 10 samples over depth intervals on the order of 100 m characterizes thermal conductivity sufficiently, considering the other sources of error. Additional detail regarding heat-flow calculations for individual wells are given below.

US7: This well was drilled for purposes other than heat flow, and no systematic sample collection was made during drilling. The six samples were scooped off the ground surface near the wellhead so that no depth could be assigned to individual samples, and no thermal conductivity profile is shown in Figure 2. Significant stratification is evident in the gradient profile (Figure 2), and the apparent gradient falls off markedly below 800 feet. Our heat-flow calculation is based on the harmonic mean thermal conductivity and the least-squares gradient between 400 and 800 feet.

PSA: This well was drilled on the southwest side of the San Andreas fault (Figure 1) in a porous sandstone of the Punchbowl Formation. Based on information from cores and outcrop samples, we estimated a porosity of 20% and adjusted the measured grain conductivities accordingly.

PSB and PSBB: PSB was drilled in 1977 as part of a regional stress/heat-flow study. PSBB was drilled later to obtain deeper stress data. Heat-flow calculations over two intervals in PSB are in reasonable agreement, but in neighboring PSBB, temperature gradients decrease systematically to depths greater than 1000 feet (300 m) strongly suggesting a local hydrologic effect.

Heat-flow calculations for PSBB are summarized in Table 2. Corrections were made for the variation of in situ conductivity with temperature (the lab measurements were made at ~25°C), but it is seen from the table that these corrections are trivial. It also is seen from the table that heat flow varies systematically in the upper 300 meters with an average of about 80 mWm^{-2} below this depth. This is in contrast to our mean value of 65 mWm^{-2} for PSB. Comparison of the last profile from the original hole and the upper 400 meters of the new hole, Figure 6, suggests a probable cause for the systematic variation in the upper 300 meters of PSBB. Temperatures in PSBB are very similar to those of PSB to a depth of about 250 feet. Below this, they are systematically lower and increasingly so to the depth of the old hole. The original hole was cased to total depth, and the new hole has casing to nearly the same depth; in neither case was the casing grouted in. From the difference in temperature profiles, it is apparent that the hydraulic head decreases with depth in PSBB and that over considerable depth we have a slow, downward percolation of water. Qualitatively, this has the effect of lowering the gradients in the upper part of the hole and increasing them with depth. Consequently, the heat flow below 300 meters, though internally

consistent, cannot be interpreted as the regional heat flux. The average of all component heat flows, 74±3 mWm^{-2} is about 10% higher than the value published for PSB. Whether this mean is regionally representative depends, to some extent, on how we model (quantitatively) the hydrologic regime within the hole. An understanding of the measurable physical processes occuring within this hole probably requires that we look in some detail at temperature profiles in an attempt to determine just where the water is leaving the well.

Some further insights into the thermal-hydrologic regime of this borehole may be gleaned from a study of three profiles (Figure 7), two from PSBB, and the last profile from PSB (shown in more detail in Figure 6). Among these are:

1) Temperatures in PSBB are in equilibrium. Two logs obtained nine months apart are identical, confirming that the latest temperature profile represents the equilibrium formation temperature perturbed by whatever quasi steady-state hydrologic processes are occurring in the borehole.

2) The lowermost 100 or so meters of the profile from PSBB could have been predicted by extrapolation of the bottom portion of the last profile in PSB. This, in turn, suggests that the water moving downward in the hole is exiting at various permeable zones within the hole, and that we have very nearly regained the steady-state, conductive regime near the bottom of the hole.

PSC, BBUT: Another pair of wells were drilled near Black Butte. The first well (PSC) was drilled to a little over 700 feet (Figure 8). No unusual constituents were detected in the cuttings that would explain the spikes in the gradient profile at depths of about 300 and 450 feet (Figure 8). These could be the result of thin poorly conducting layers, or lateral water flow in thin, permeable zones. In neither case do they have a significant effect on the heat-flow calculation. As with PSB-PSBB, the deeper well has a systematically increasing gradient with depth, in the case of BBUT extending to a depth of about 400 feet (122 m, Figure 9). Once again, this can most probably be attributed to local vertical downflow of water. In this case, the mean heat flows for the two wells are in reasonable agreement (Table 1) as are the component heat flows below 122 m in BBUT (Table 3). The heat flows agree even though local variability results in a nearly 2°C displacement between the two profiles (Figure 10). The two wells are essentially at the same elevation, topographic effects are negligible, and the collars are only 1 km apart. The displacement between profiles would thus seem to arise from local lateral variability in albedo or some other microclimatic effect.

PSD: The temperature profile in PSD exhibits some inexplicable irregularities (Figure 11), but the average gradient between about 370 and 640 feet is reasonably consistent although there is a suggestion of an increase in gradient with depth.

PSE, HVI: These two wells were also drilled at the same location. Once again, the temperature profiles vary in detail (Figures 12 and 13), but there is no evidence for systematic gradient variations and heat flows from the two wells are in good agreement (Table 1).

HIVS: Another moderately deep well was drilled some 10 km west of the previous pair. The gradient increases with depth below the water table (Figure 14), but conductivity decreases proportionally resulting in a constant heat flow to within the uncertainty of the measurements (Table 1). Sufficient material was not available to prepare samples for radiometric measurements.

PSF: This well was originally 670 feet deep but was bridged at about 370 feet when logged (Figure 15). There are only two conductivity values averaging about 3 $Wm^{-1} K^{-1}$ in the gradient interval. In this instance, we judged that the entire conductivity sample would be more representative of the gradient interval than these two values, so the average of all 11 conductivities was used in the heat-flow calculation (Table 1).

CCT: The temperature profile (Figure 16) is curved indicating a systematic increase in gradient between about 22°C/km at 100 feet to nearly 30°C/km at the bottom. The only plausible explanation for the observed curvature is downward water flow. In this case, the best estimate of heat flow is the product of the least-squares gradient and harmonic mean conductivity (Table 1). The value of 69 mWm^{-2} should be considered a lower limit, however.

KJN: This shallow well (Figure 16) poses no particular problem in interpretation.

CAJN: The thermal regime of this well (Figure 18) has been discussed elsewhere (Lachenbruch and others, 1986a, b). These papers discuss the ambiguity in the heat flow of the upper ~1.8 km because of the effects of poorly determined porosity in sedimentary material, uplift, erosion and refraction. These result in a large uncertainty in the value for regional heat flux. We here tabulate component heat flows at 1000 ft (305 m) intervals (Table 4), apply a topographic correction, and use the analytical models of Lachenbruch and others (1986b) to estimate the "most probable" values for equilibrium heat flow. The effects of steady-state local terrain and Pleistocene uplift are of the same magnitude and of opposite sign (Table 4). The gradient correction is thus dominated by the effects of erosion during the past million years or so. Porosities of 9 outcrop samples of the sedimentary rocks range from about 6% to over 20% (Table 5) with a mean of 11.2±5% (S.D.). "Uncorrected" heat flows, assuming an implausible zero porosity for the Crowder and Punchbowl formations exhibit no systematic variation with depth and average 98±3 mWm^2. Using corrected gradients and the zero porosity assumption results in a somewhat lower heat flow for the upper 305 m than for the remainder. We believe, however, that the porosity of 11.2±5% is the most plausible assumption for the sedimentary material. This results in a mean heat flow of about 60 mWm^{-2} in the sandstone and about 78 mWm^{-2} in granite. The exact configuration of the contact between granite and sandstone is not known, but from surface observations it seems likely that the dip is at least 45°. The companion paper (Lachenbruch and others, 1986b, Figure R-4) shows two extreme configurations that would allow the regional heat flow to be either of the two values. These extreme configurations are unlikely but neither can be completely ruled out based on what is now known. Based on the extreme values, the most likely value for regional heat flow at this site is 69±9 mWm^{-2}, consistent with other determinations in this region (Lachenbruch and others, 1986b, Figure 3).

The uncertainty estimate is low because it does not include the uncertainty in the corrections to the gradient, and for the sedimentary rocks, the uncertainty in the porosity.

GMC: This well (Figure 19) provides a straightforward determination of heat flow with a slight upward correction for steady-state topography (Table 1).

STD: The Stoddard Mountain well (Figure 20) also provides data that can be interpreted simply.

GRADIENT WELLS

Temperature profiles from eight additional wells in the region are shown in Figures 21 through 28. These wells were selected primarily as observation wells by T. L. Henyey and his associates at University of Southern California. No rock samples and, in some instances, no lithologic information were available for these wells. We have listed the least-squares gradients and, as an exercise, a range of heat flows corresponding to a plausible range of thermal conductivity for the appropriate lithology in Table 6. With the exception of US8, a very shallow well with a thermal profile obviously disturbed by water flow, all heat-flow estimates are within the range determined from the heat-flow observation wells.

DISCUSSION

The primary purpose of this report is to document some previously published and new heat-flow values near Cajon Pass (Figure 1). The previous sections, Figures 2 through 28, and Tables 1 through 6 should allow the critical reader to make his or her own judgment of the quality of the data from individual wells and of the appropriateness of our interpretation of the data. In this section, we make some observations concerning the entire data set, particularly as regards the relation between heat flow and radioactivity, and heat flow as a function of the mean depth of determination.

The present data set is largely compatible with the results presented by Lachenbruch and Sass (1980) wherein the average for region 7 (the Mojave Block) was about 68 mWm^{-2} with no peaked anomaly near the fault. The area studied in Figure 1 is not entirely coincident with region 7 and includes a few more points. The average of the 22 values from Table 1 is 67±2(SE) with once again, no peaked anomaly near the fault. Because of the various factors already discussed, the possible range at CAJN is very large, but based on the most plausible values for the effects of topography, uplift and erosion, and a position midway between the extremes on refraction (the most poorly determined disturbance) the mean value of 69±9 for CAJN is compatible with previous results.

Heat flow versus radioactivity. Heat flow is shown as a function of radioactivity in Figure 29. As has been shown for most of the Basin and Range province (Lachenbruch and Sass, 1977, 1978; Lachenbruch and others, 1985) there is no simple relation between these two quantities. The original relations for the Basin and Range and Sierra Nevada provinces are shown for reference in Figure 29. For this data set, the correlation is extremely poor ($R^2 = 0.004$) with an intercept of 70 mWm^{-2} and a slope of -0.5 km as opposed to +10 km for the relations depicted in Figure 29. Considering the complex geologic history of this region, we should not be surprised that no relation between heat flow and near-surface radioactivity can be defined.

Heat flow versus depth of measurement. Figure 30 illustrates the variation in heat flow with mean depth of determination for sites within 10 km of the San Andreas fault (no detectable variation exists for sites greater than 10 km from the fault). A close examination of Figure 30 indicates a marked depth-dependence to a depth of ~500 m and scatter about a mean of between 75 and 80 mWm^{-2} below that depth. However, it should be noted that the deeper information all comes from two holes; one (CAJN) with uncertain corrections, and the other (PSBB) with evidence of local hydrologic disturbance. In general, we have found that where there are pairs of shallow and deep wells (PSB and PSBB, PSC and BBUT, PSE and HVI), there is no or little indication of hydrologic disturbances in the shallow well, but the shallow part of the deeper well exhibits curvature in each instance and the shallow heat flows do not agree. We suggest that for the shallow wells (which are mostly above the water table), we are able to measure regional heat flux to within ±10-15% but when we drill an intermediate depth well (~1 km) the upper 200 to 300 meters tends to be disturbed by downward water flow under the influence of slight head gradients in highly fractured and hence, very permeable rock to depths of 150 to 200 m. Heat flow might

also be affected by a climatic disturbance with surface amplitude of 1 or 2 degrees which was initiated during the past 50 to 150 years. This might be responsible for a systematic lowering of the regional heat flux on the order of 10% in the upper 150 to 200 m, within which depth range the majority of heat-flow determinations in southern and central California have been made.

A combination of hydrologic, structural and climatic effects might be distorting the shallow thermal regime of the San Andreas fault zone and surrounding areas, as suggested in Figure 30. It appears unlikely, however, that this distortion will have a major impact on the interpretation of heat-flow measurements in this region.

Acknowledgments. We are grateful to Fred Grubb and Bob Husk for making field measurements and collecting samples and E. P. Smith for conductivity measurements. We are indebted to Don Stierman for making the samples from HVIS available to us and to A. R. Smith for determinations of radiogenic heat production.

References

Brune, J. N., Henyey, T. L., and Roy, R. F., 1969, Heat flow, stress, and rate of slip along the San Andreas fault, California: Journal of Geophysical Research, v. 74, p. 3821-3827.

Henyey, T. L., 1968, Heat flow near major strike-slip faults in California, Ph.D. thesis, California Institute of Technology, Pasadena, California.

Henyey, T. L., and Wasserburg, G. J., 1971, Heat flow near major strike-slip faults in California: Journal of Geophysical Research, v. 76, p. 7924-7946.

Lachenbruch, A. H., and Sass, J. H., 1973, Thermo-mechanical aspects of the San Andreas fault system, in Proceedings of the Conference on the Tectonic Problems of the San Andreas Fault System, p. 192-205: Stanford University Press, Palo Alto, California.

Lachenbruch, A. H., and Sass, J. H., 1977, Heat flow in the United States and the thermal regime of the crust, in Heacock, J. G., editor, The Earth's Crust, Geophysical Monograph 20, p. 626-675: American Geophysical Union, Washington, D. C.

Lachenbruch, A. H., and Sass, J. H., 1978, Models of an extending lithosphere and heat flow in the Basin and Range province: Geological Society of America Memoir 152, p. 209-250.

Lachenbruch, A. H., and Sass, J. H., 1980, Heat flow and energetics of the San Andreas fault zone: Journal of Geophysical Research, v. 85, p. 6185-6223.

Lachenbruch, A. H., Sass, J. H., and Galanis, S. P., Jr., 1985, Heat flow in southernmost California and the origin of the Salton Trough: Journal of Geophysical Research, v. 90, p. 6709-6736.

Lachenbruch, A. H., Sass, J. H., Moses, T. H., Jr., and Galanis, S. P., Jr., 1986a, Thermal studies at the Cajon Pass borehole (abstract): EOS, v. 67, p. 379-380.

Lachenbruch, A. H., Sass, J. H., Moses, T. H., Jr., and Galanis, S. P., Jr., 1986b, Thermal considerations and the Cajon Pass borehole: U.S. Geological Survey Open-File Report 86-469.

Roy, R. F., Blackwell, D. D., and Birch, F., 1968, Heat generation of plutonic rocks and continental heat flow provinces: Earth and Planetary Science Letters, v. 5, p. 1-12.

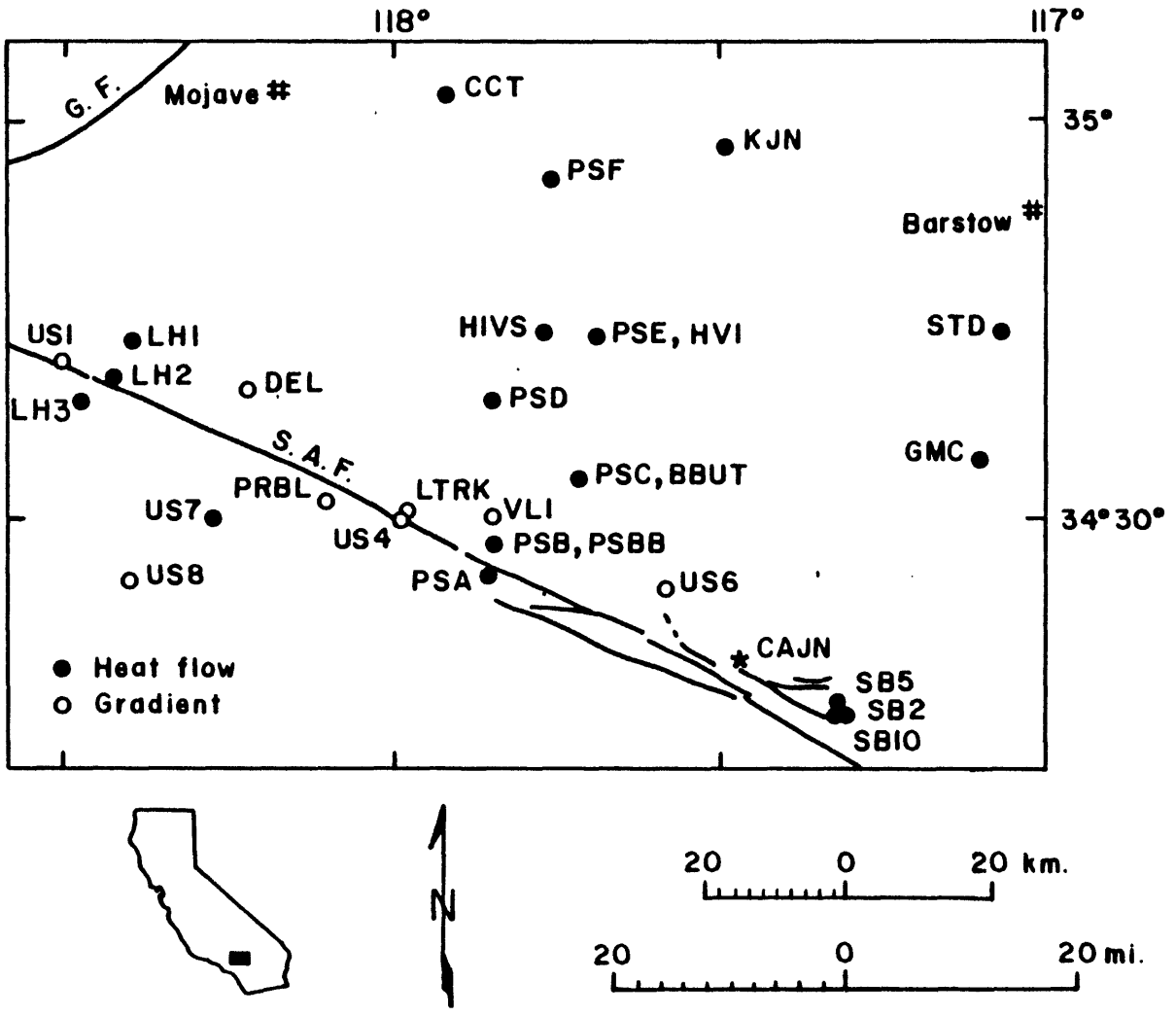

Figure 1. Map of southwestern Mojave Desert with locations of heat flow and temperature-gradient wells. Asterisk shows location of Cajon Pass site (CAJN). G.F., Garlock fault; S.A.F., San Andreas fault.

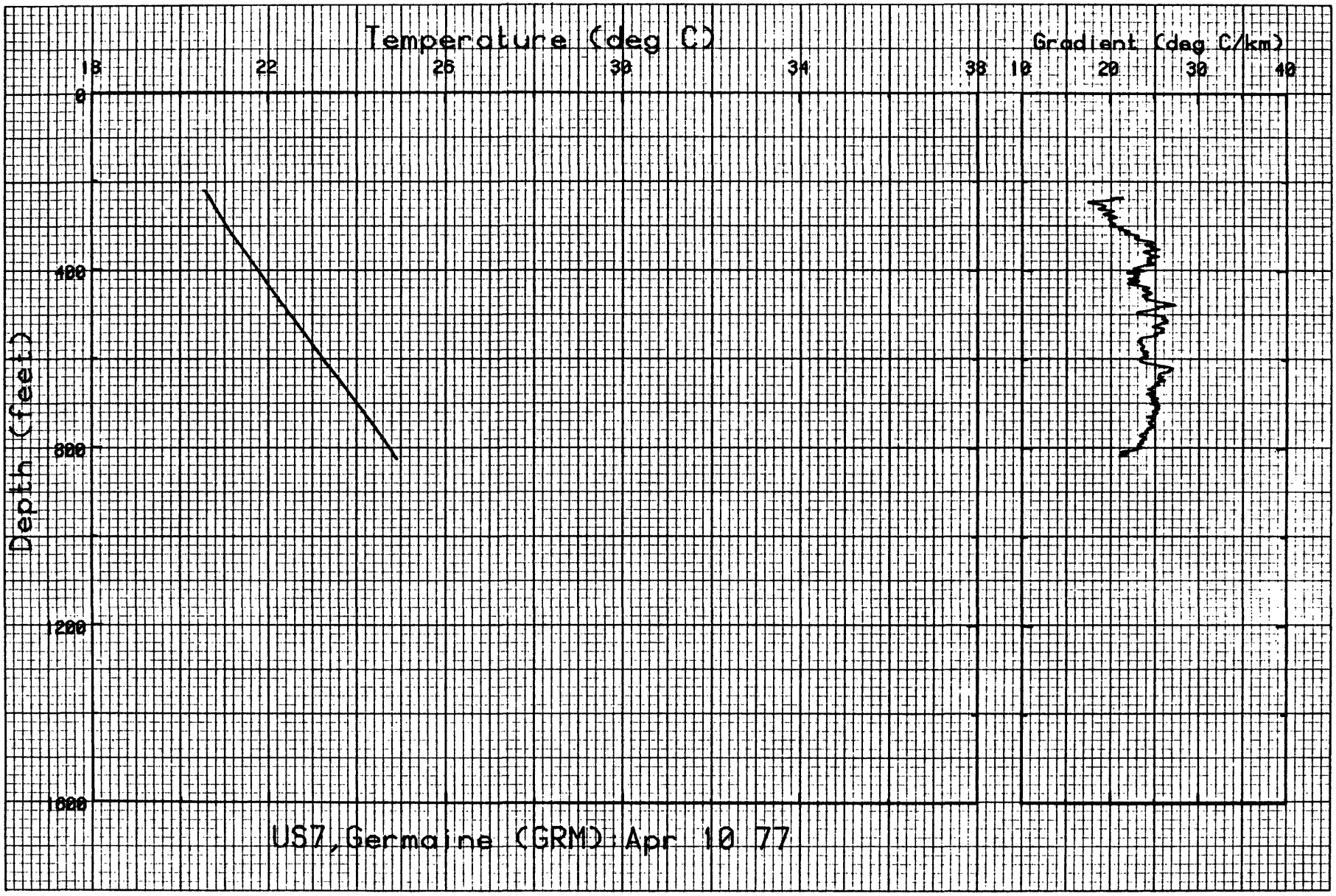

Figure 2. Temperature and gradient profiles from US7 (Germaine).

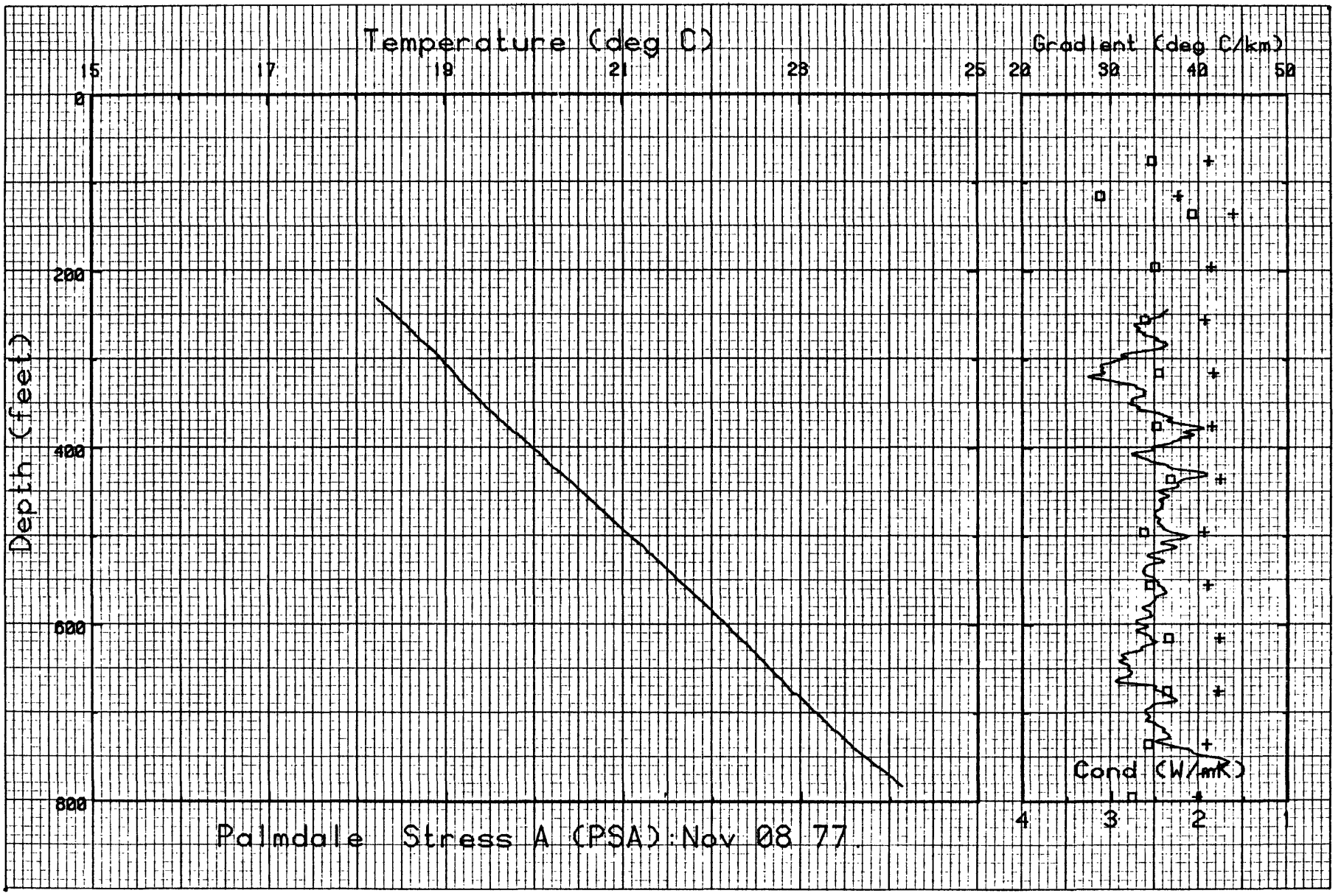

Figure 3. Temperature, gradient, and thermal conductivity profiles for PSA. Squares are grain conductivities, plus signs; formation conductivities based on an assumed porosity of 20%.

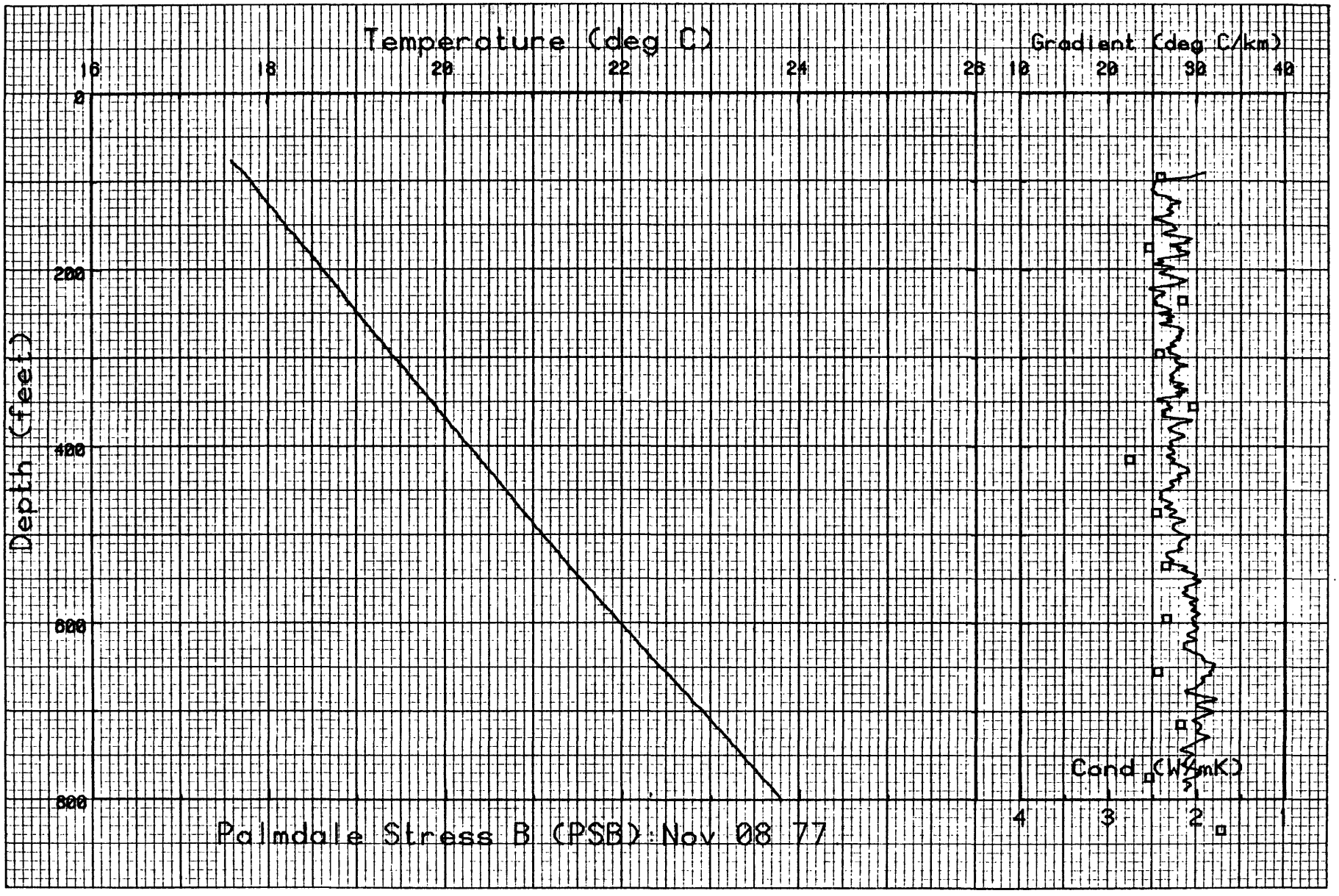

Figure 4. Temperature, gradient, and thermal conductivity profiles for PSB.

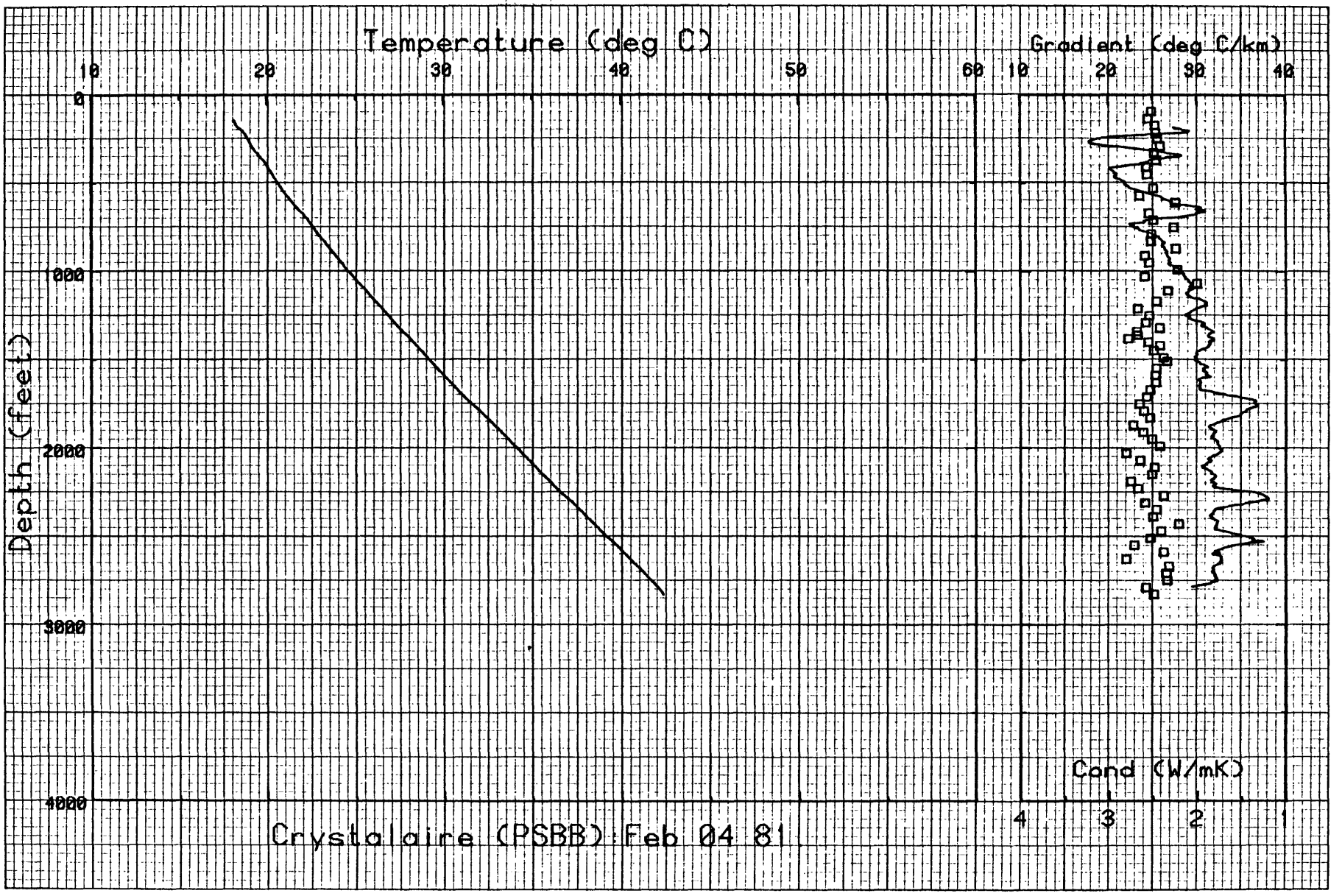

Figure 5. Temperature, gradient, and thermal conductivity profiles for PSBB.

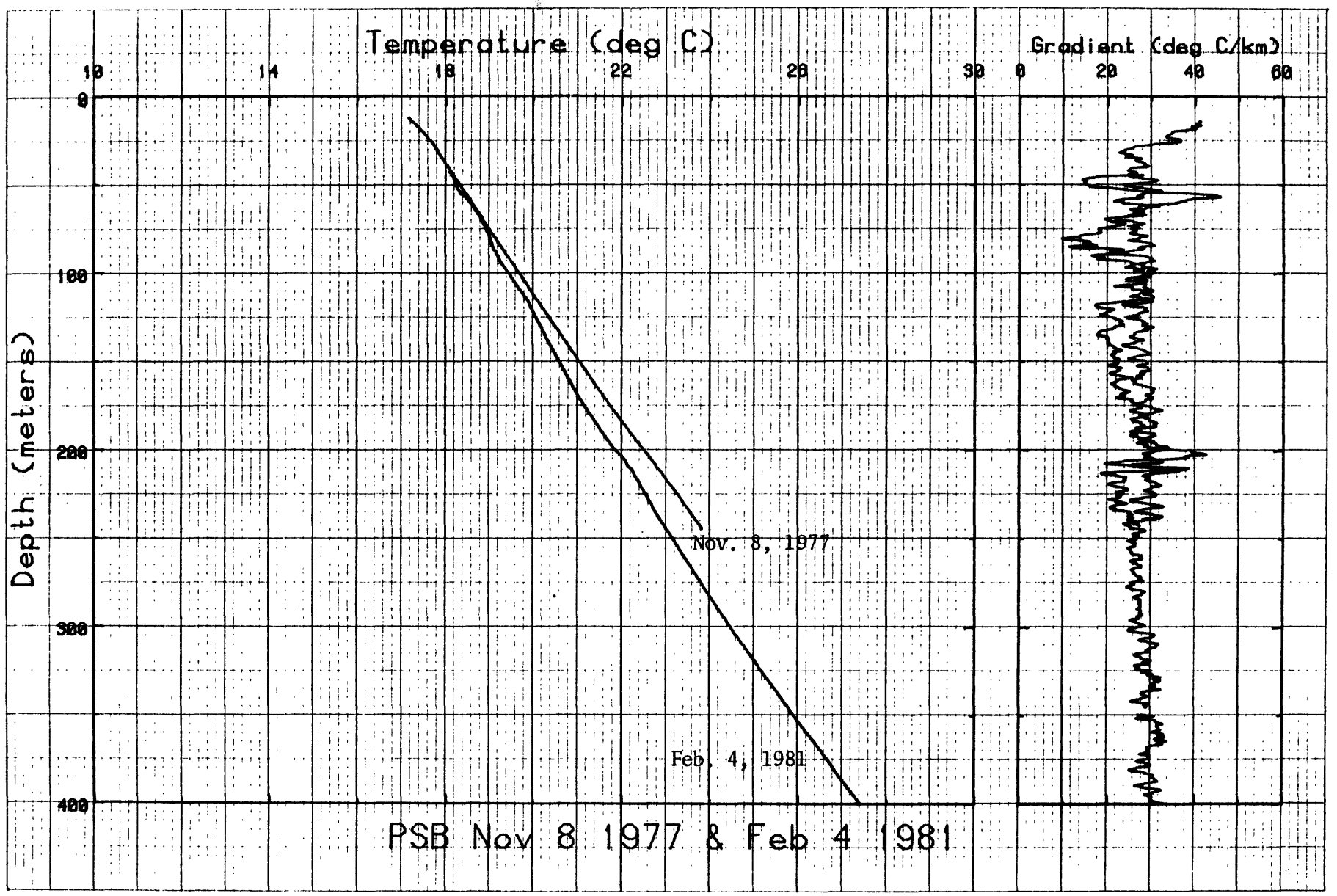

Figure 6. Temperature and gradient profiles from the original hole, PSB, and from the deeper well, PSBB, drilled on the same pad.

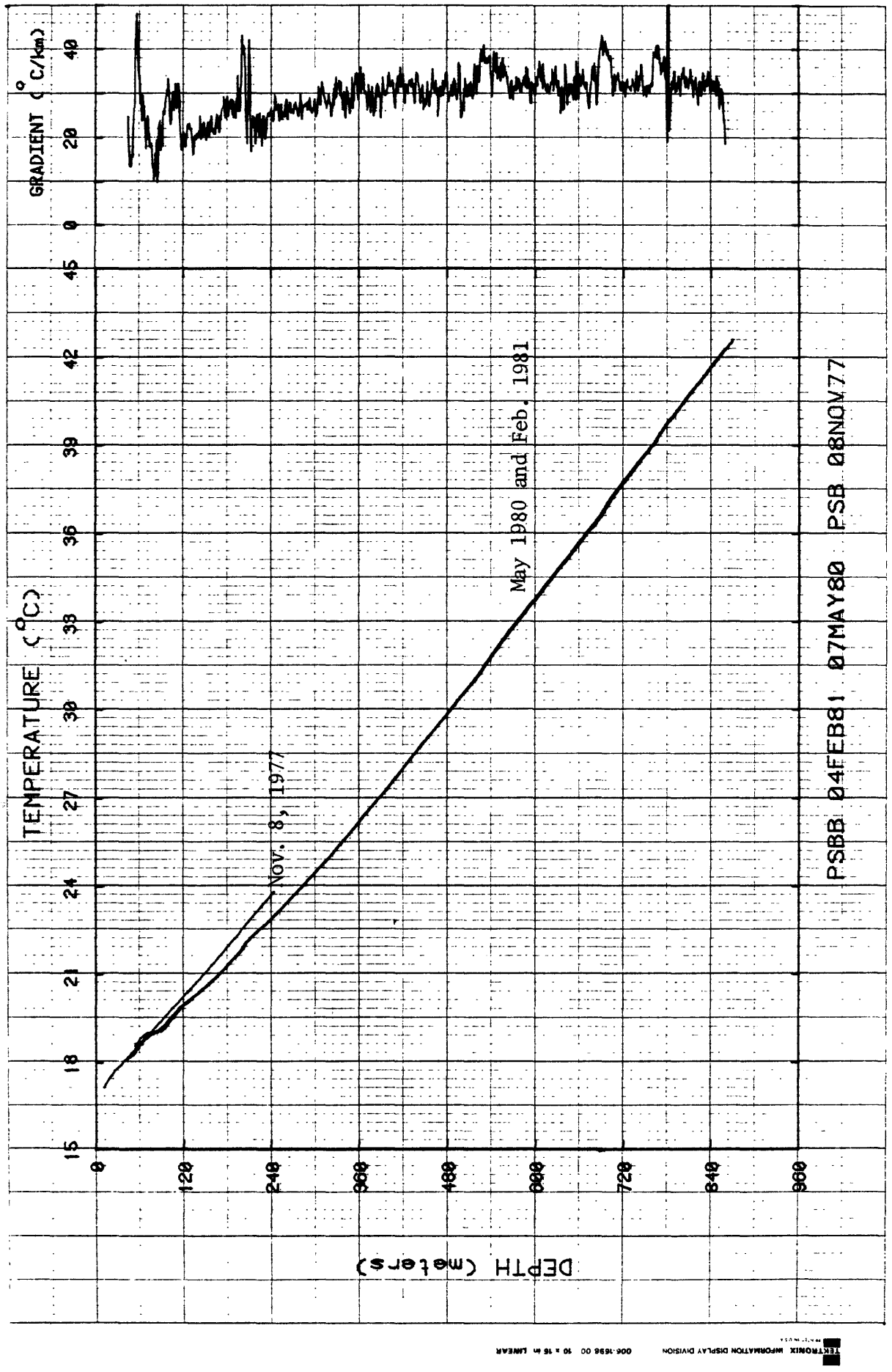

Figure 7. Temperature profiles for logs on three dates in PSB and PSBB.

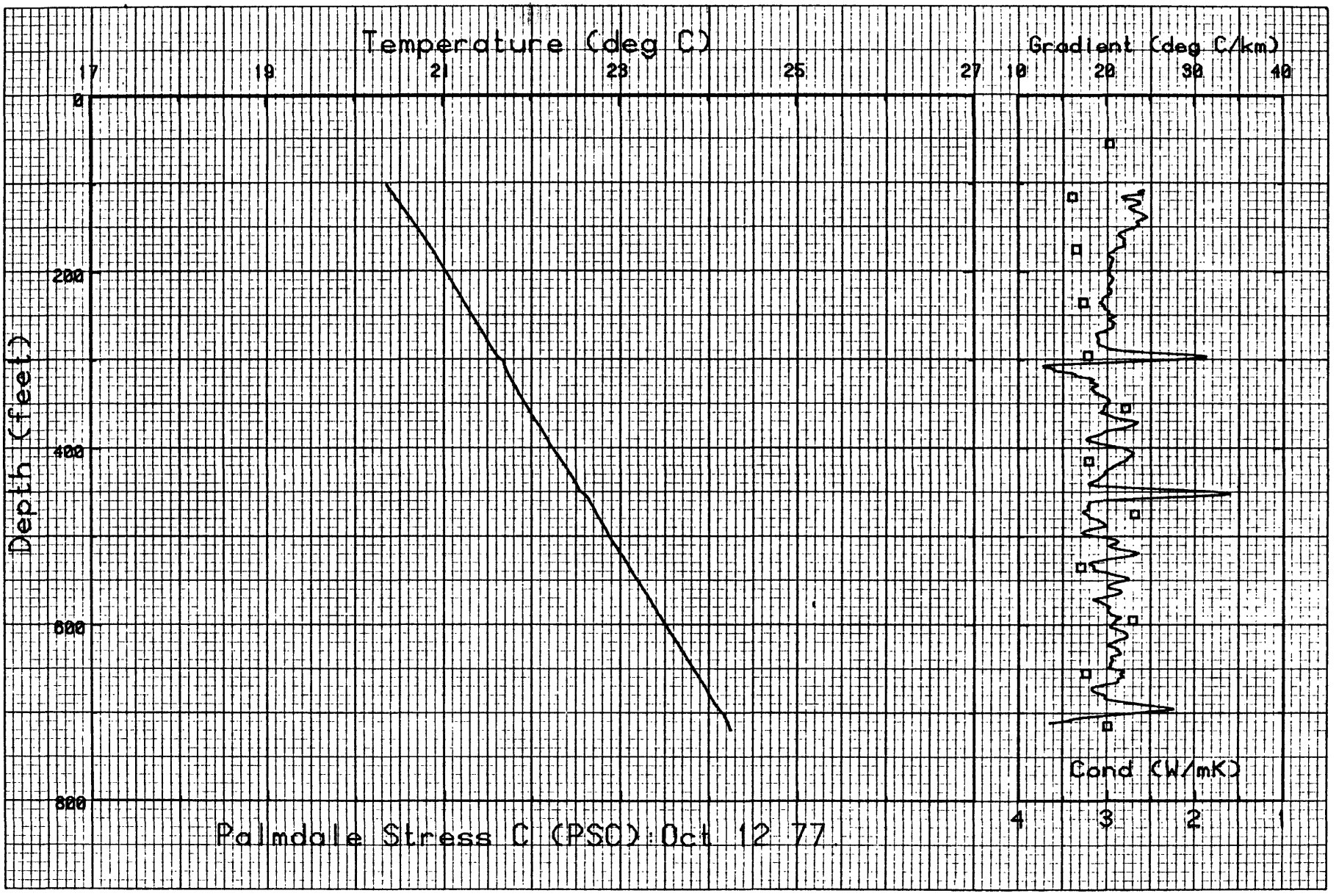

Figure 8. Temperature, gradient, and thermal conductivity profiles for PSC.

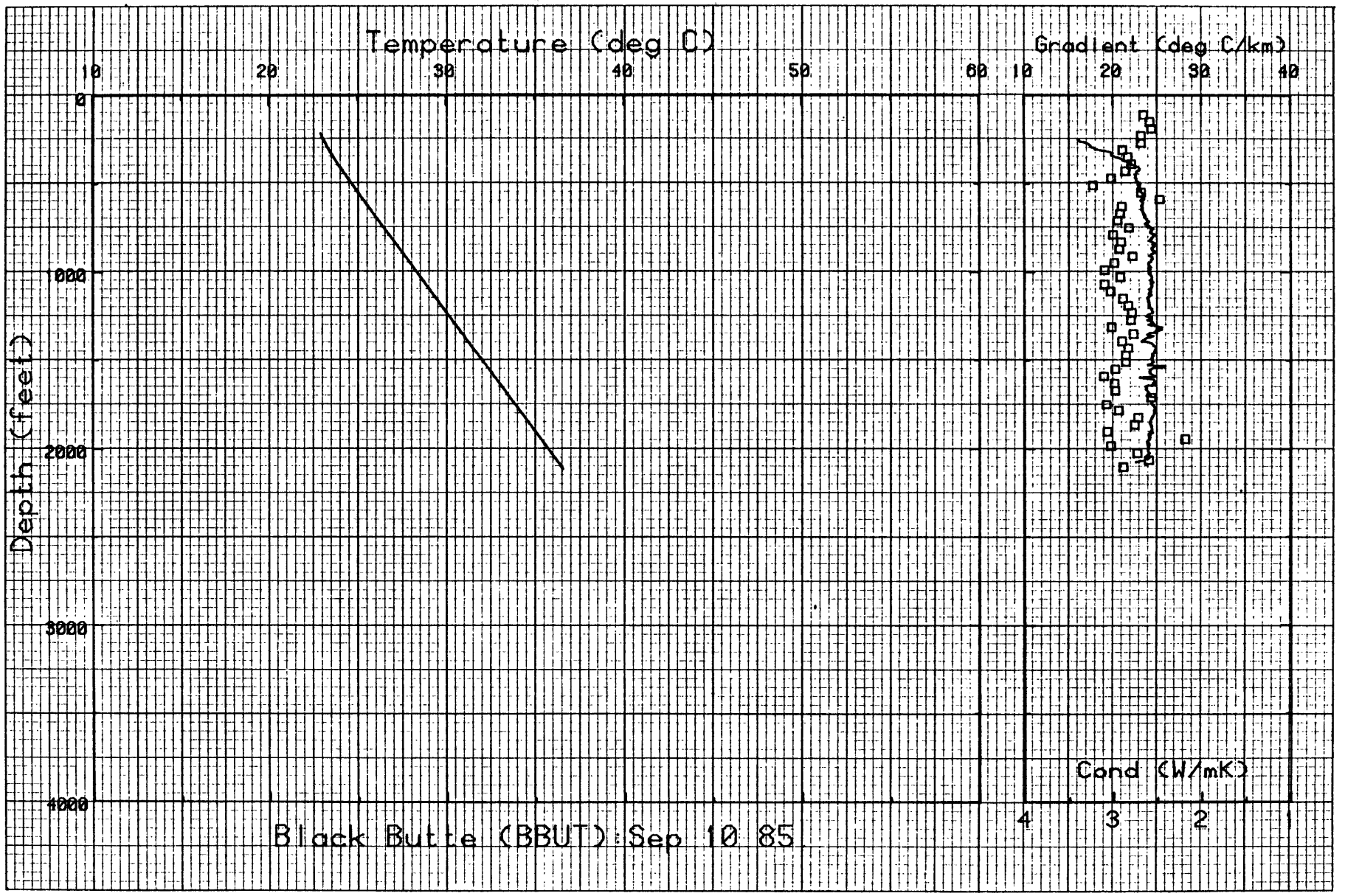

Figure 9. Temperature, gradient, and thermal conductivity profiles for BBUT.

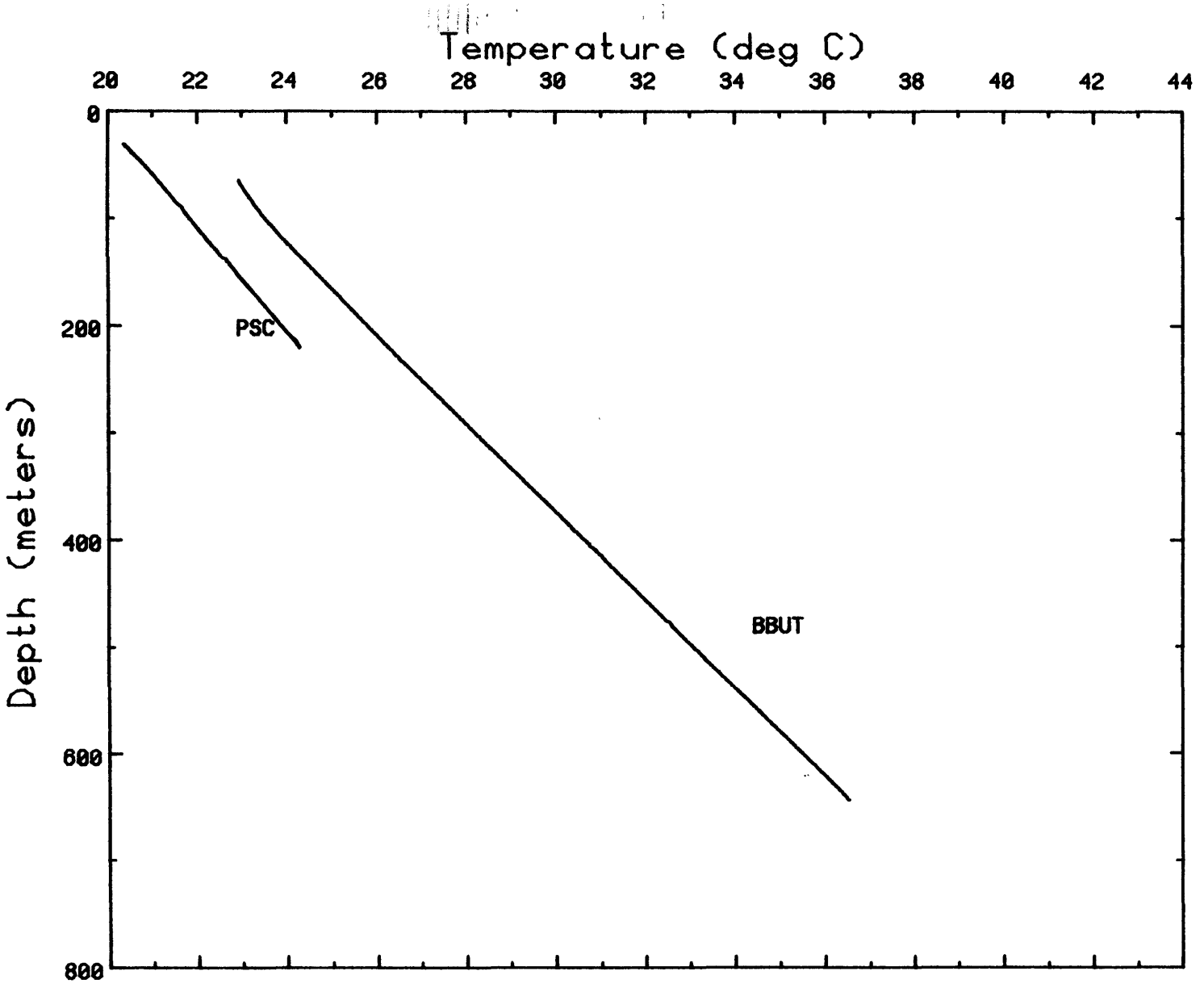

Figure 10. Temperature logs for Black Butte & PSC.

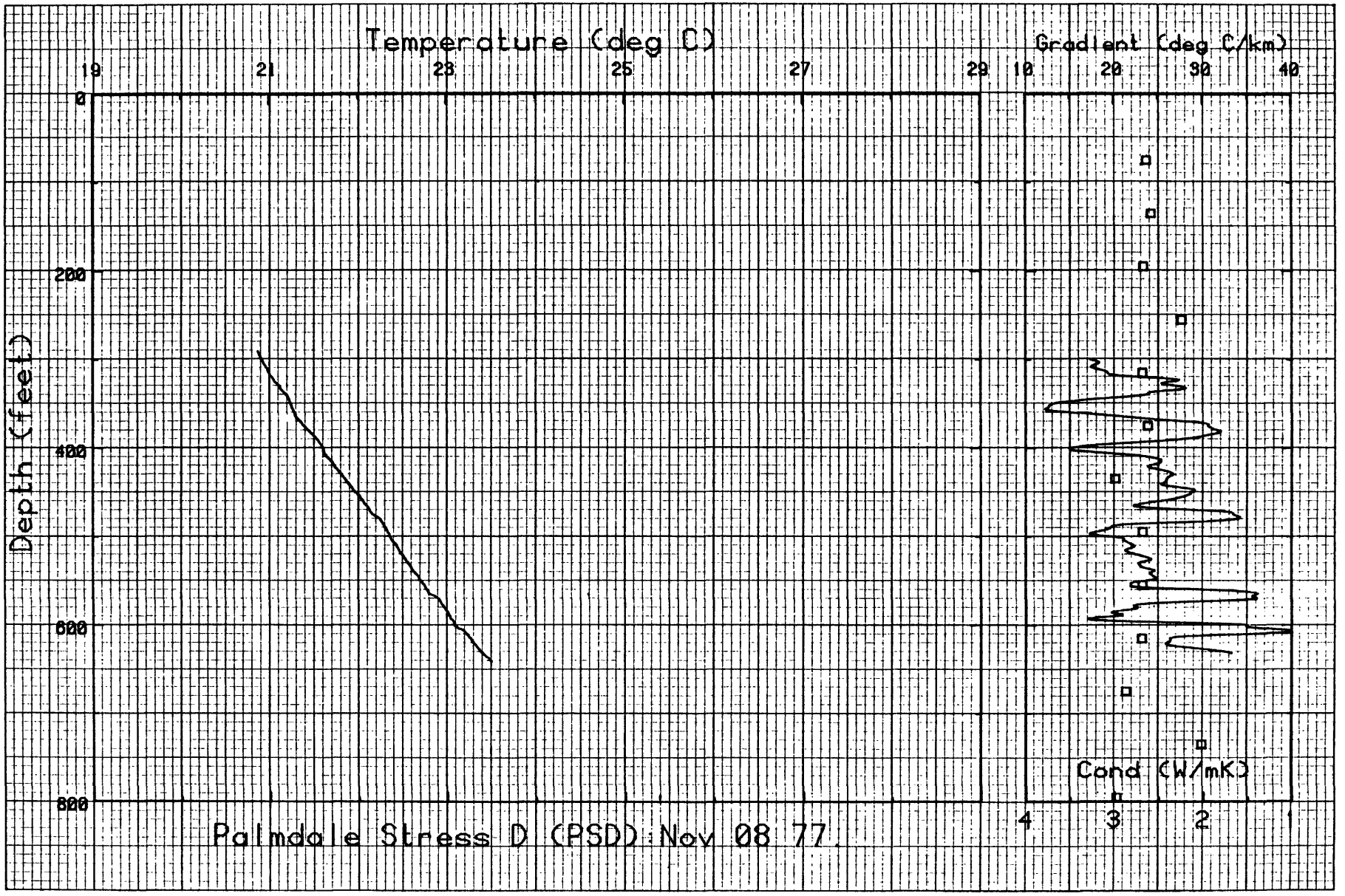

Figure 11. Temperature, gradient, and thermal conductivity profiles for PSD.

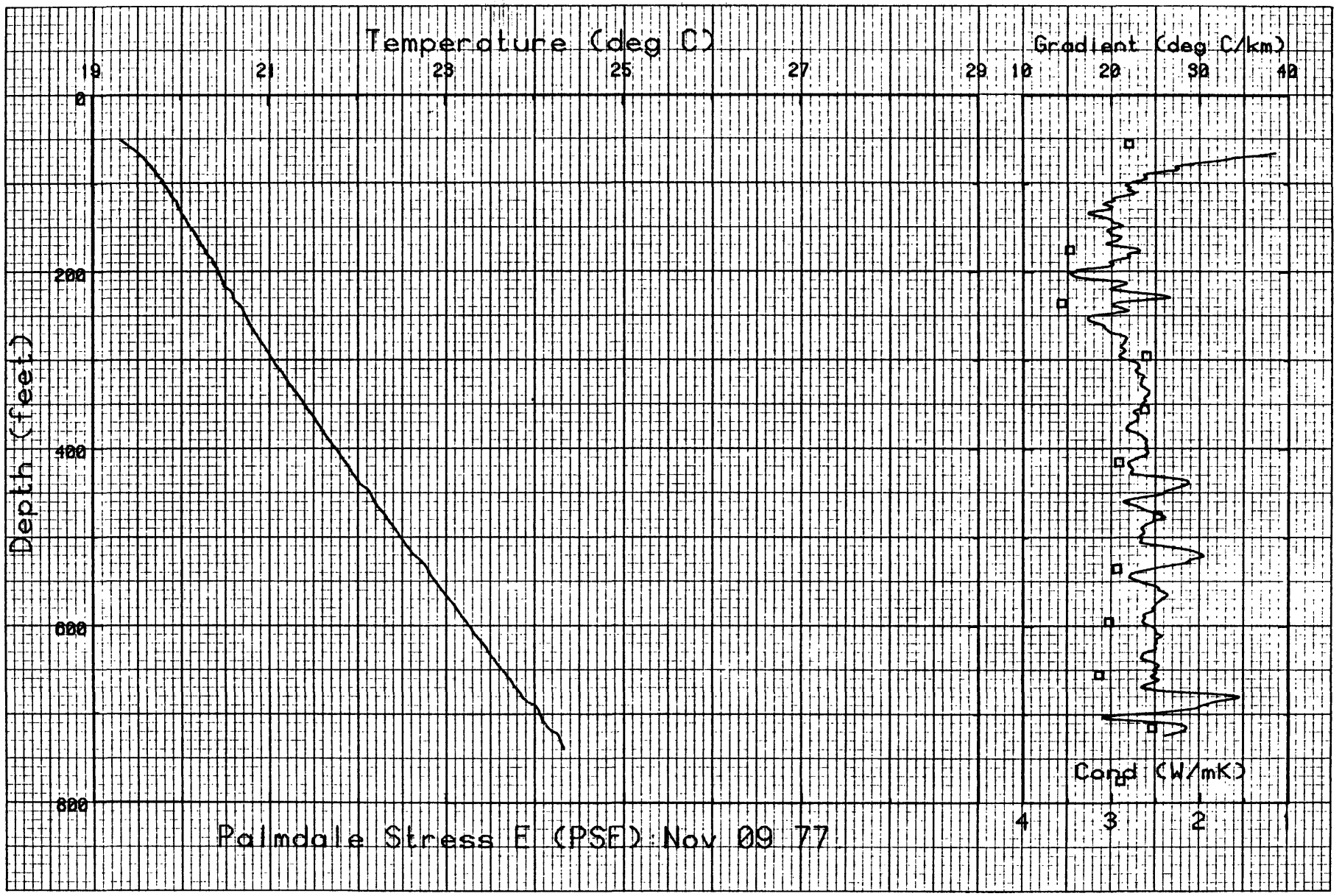

Figure 12. Temperature, gradient, and thermal conductivity profiles for PSE.

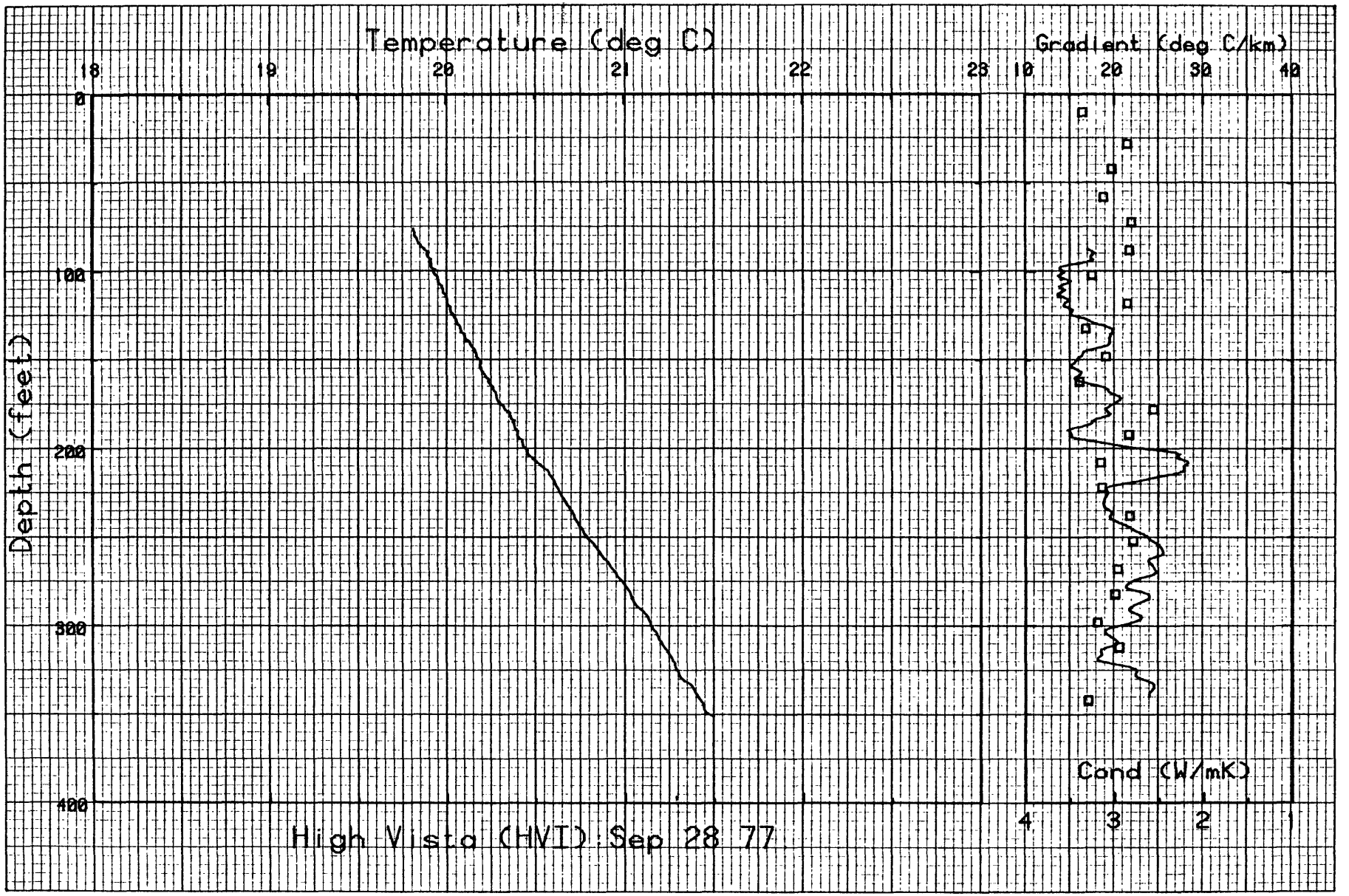

Figure 13. Temperature, gradient, and thermal conductivity profiles for HVI.

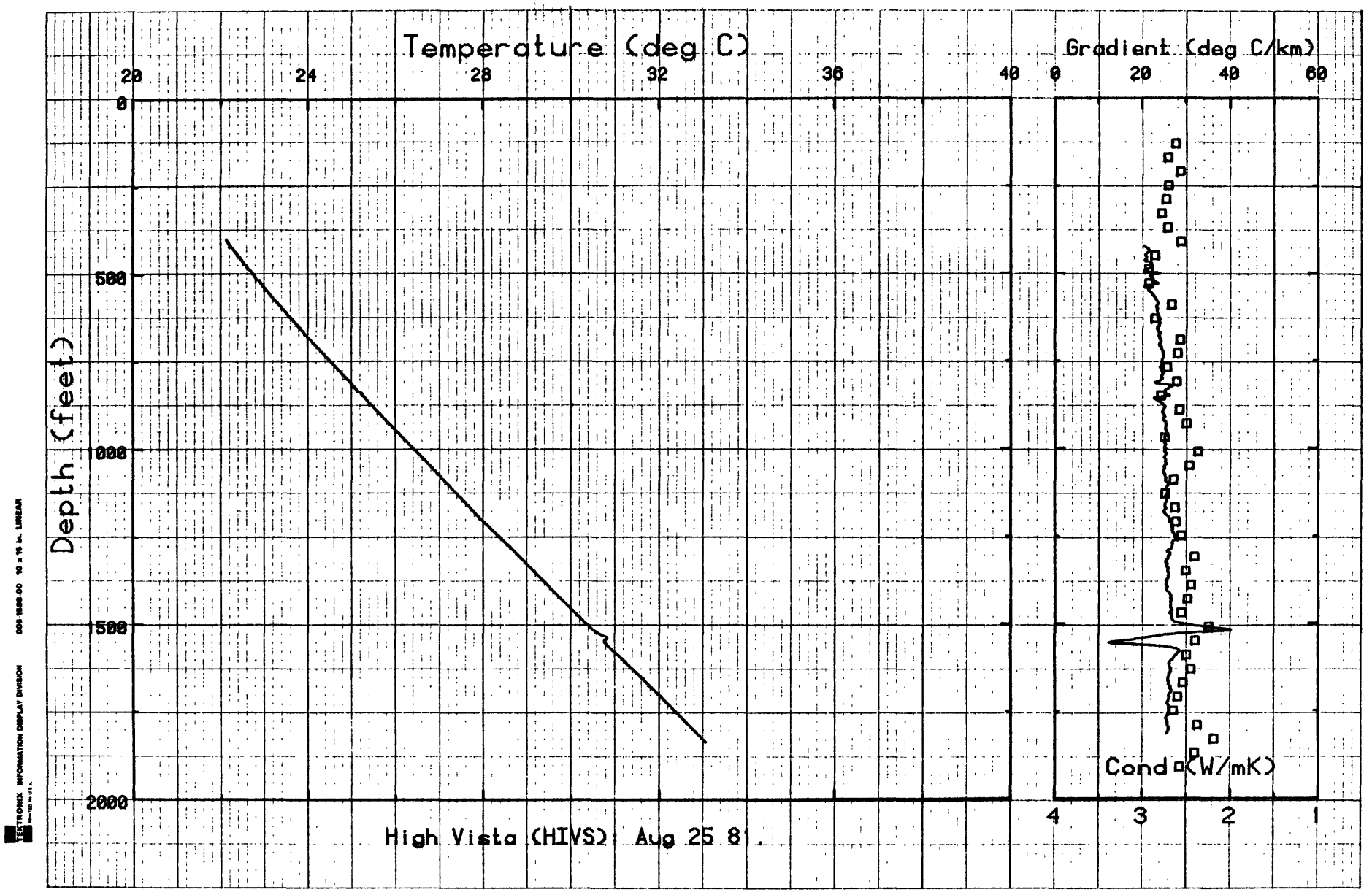

Figure 14. Temperature, gradient, and thermal conductivity profiles for HIVS.

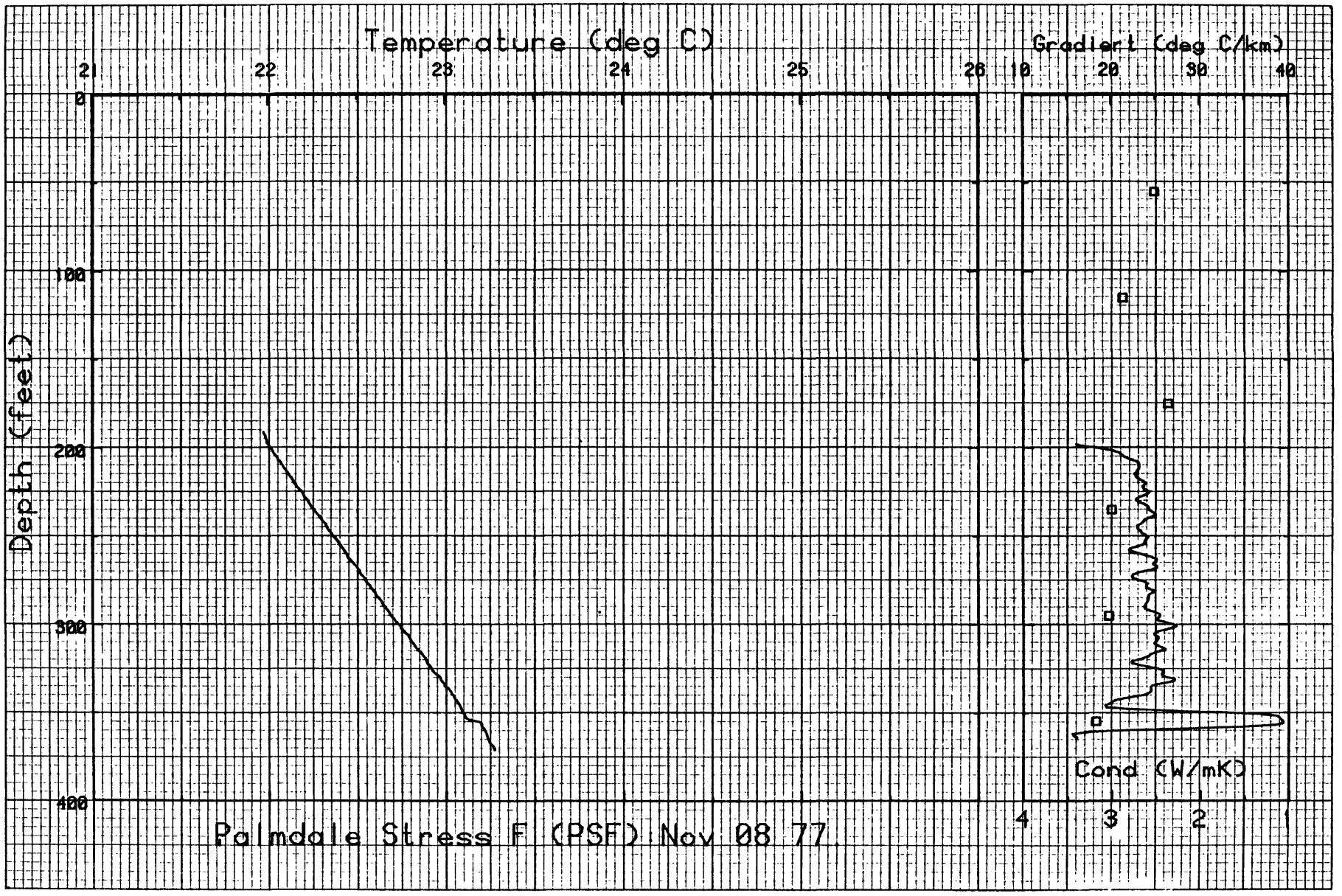

Figure 15. Temperature, gradient, and thermal conductivity profiles for PSF.

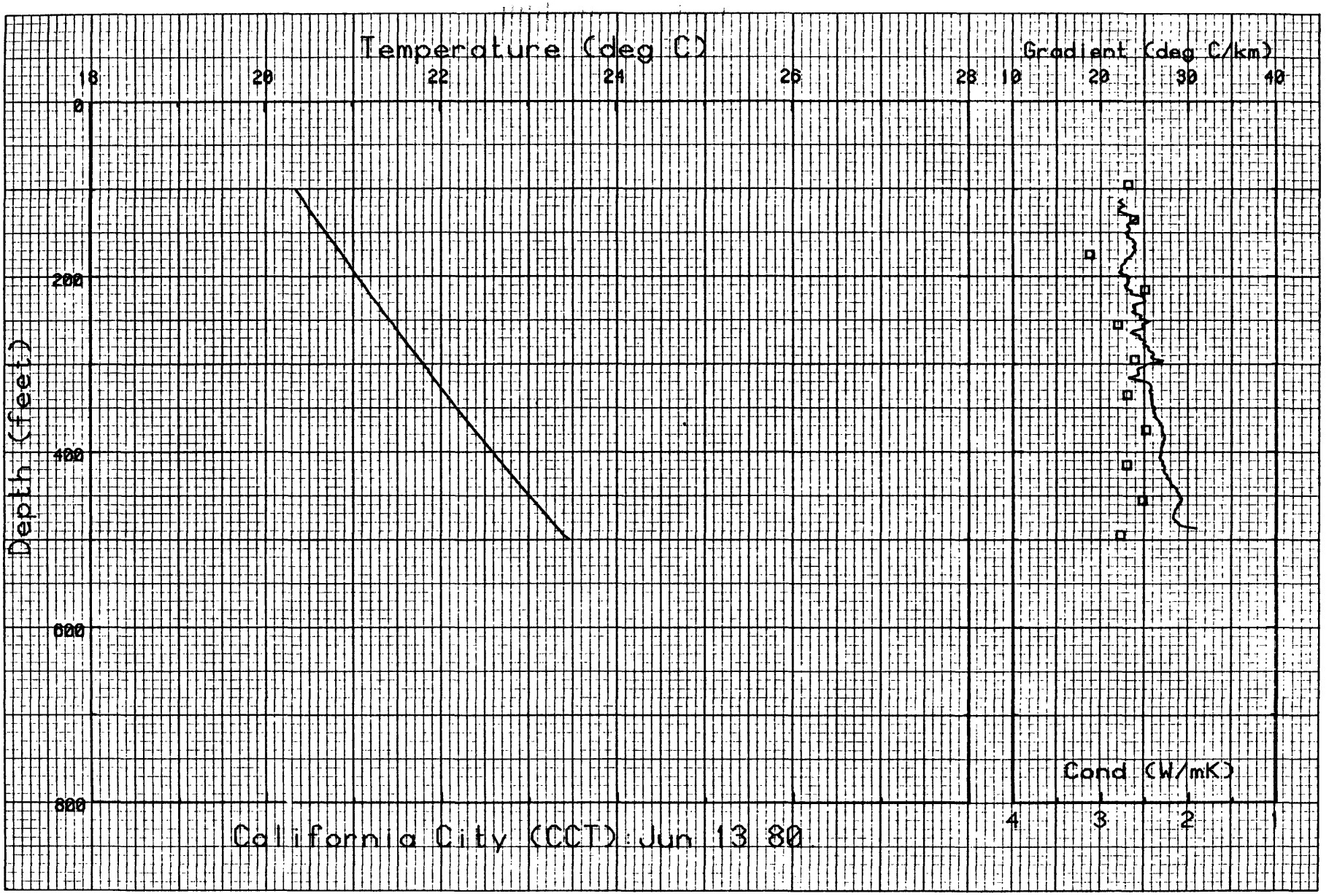

Figure 16. Temperature, gradient, and thermal conductivity profiles for CCT.

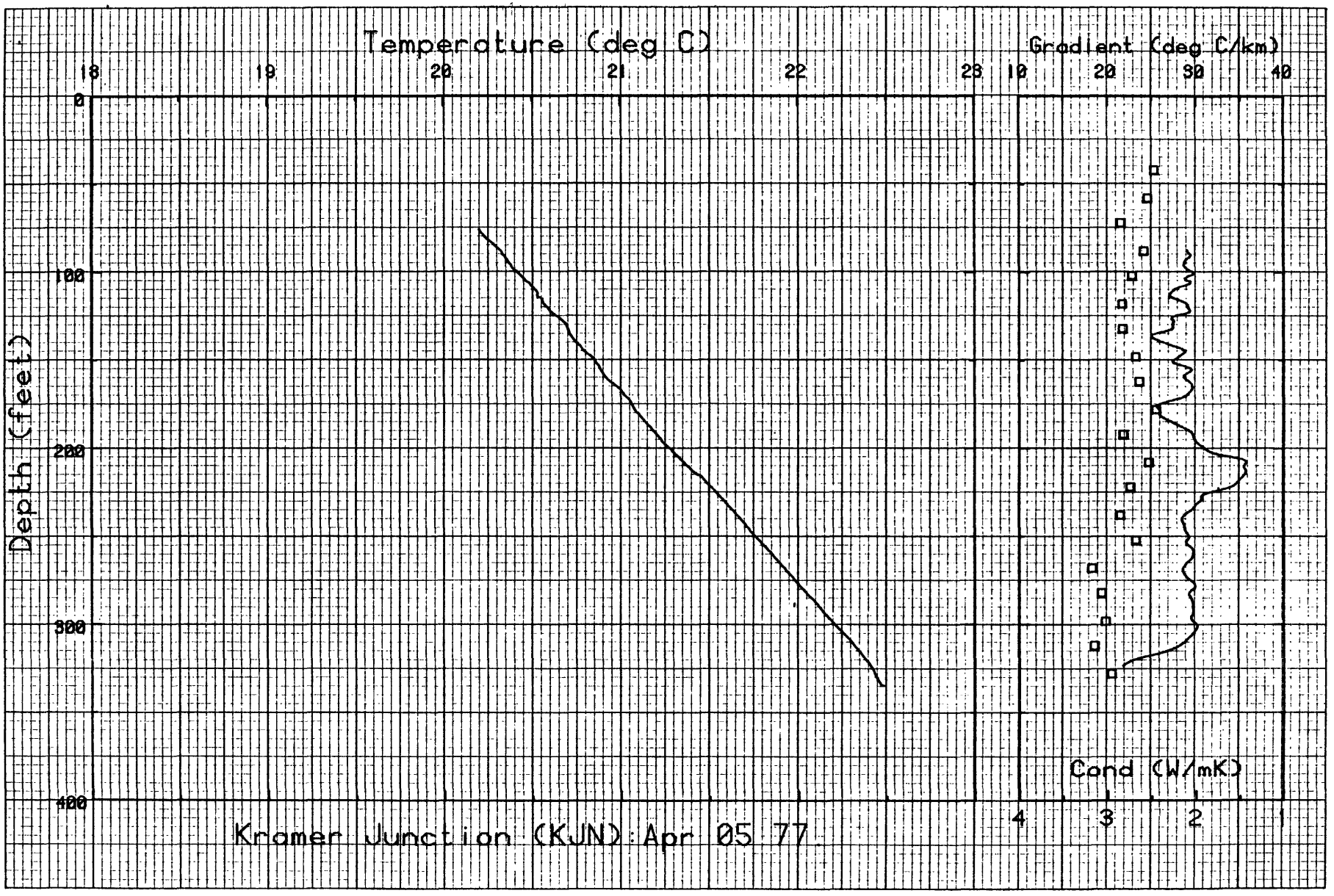

Figure 17. Temperature, gradient, and thermal conductivity profiles for KJN.

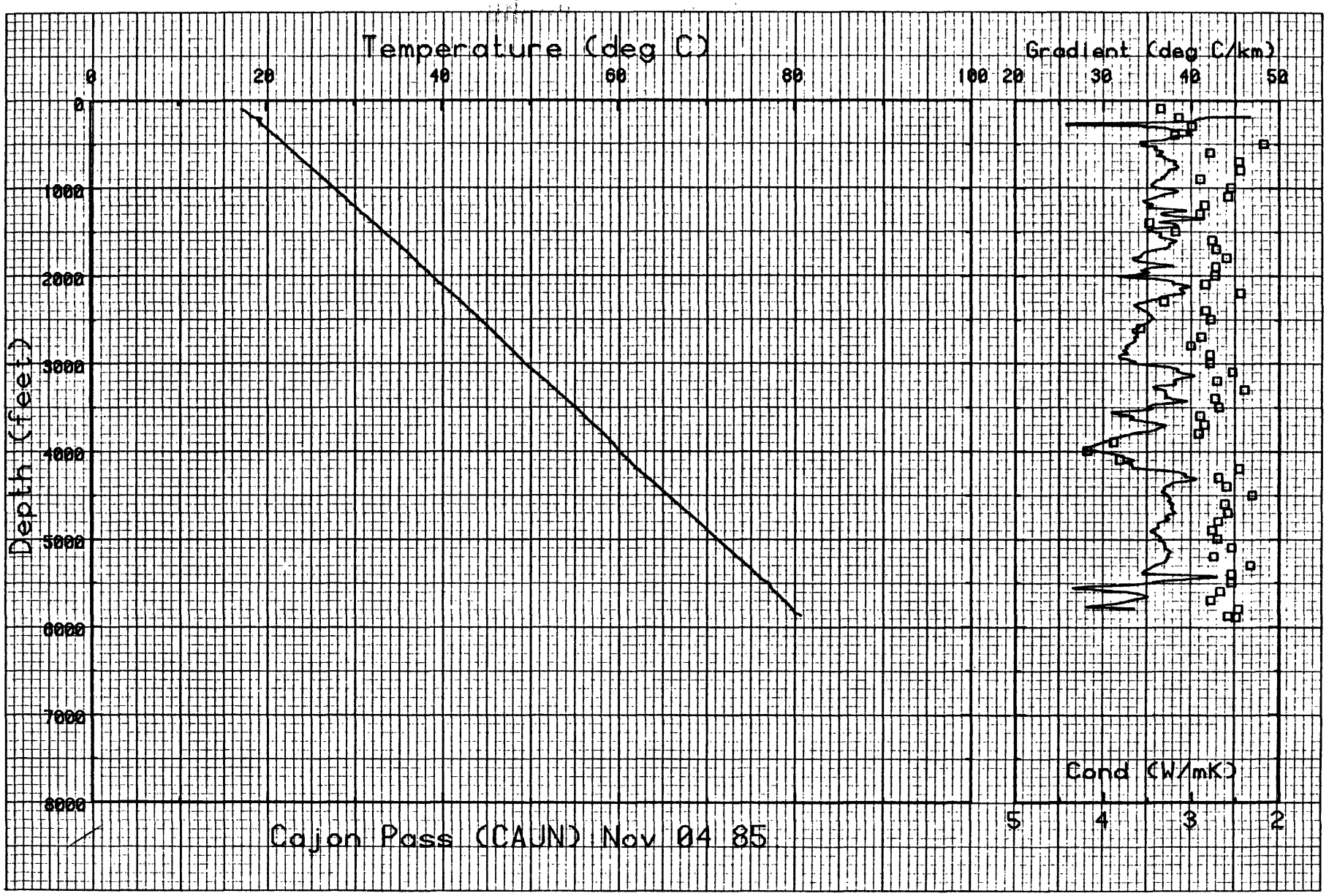

Figure 18. Temperature, gradient, and thermal conductivity profiles for CAJN.

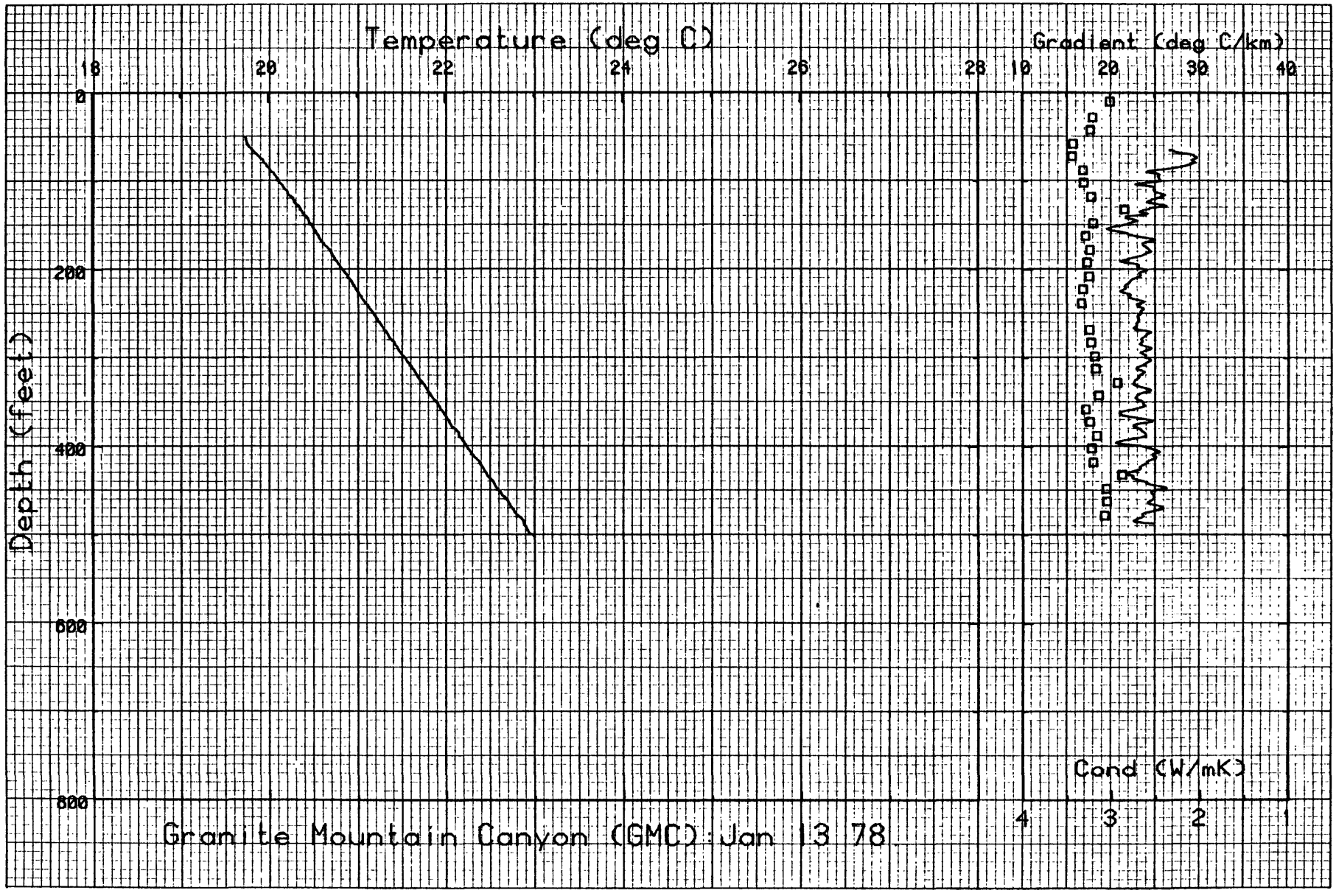

Figure 19. Temperature, gradient, and thermal conductivity profiles for GMC.

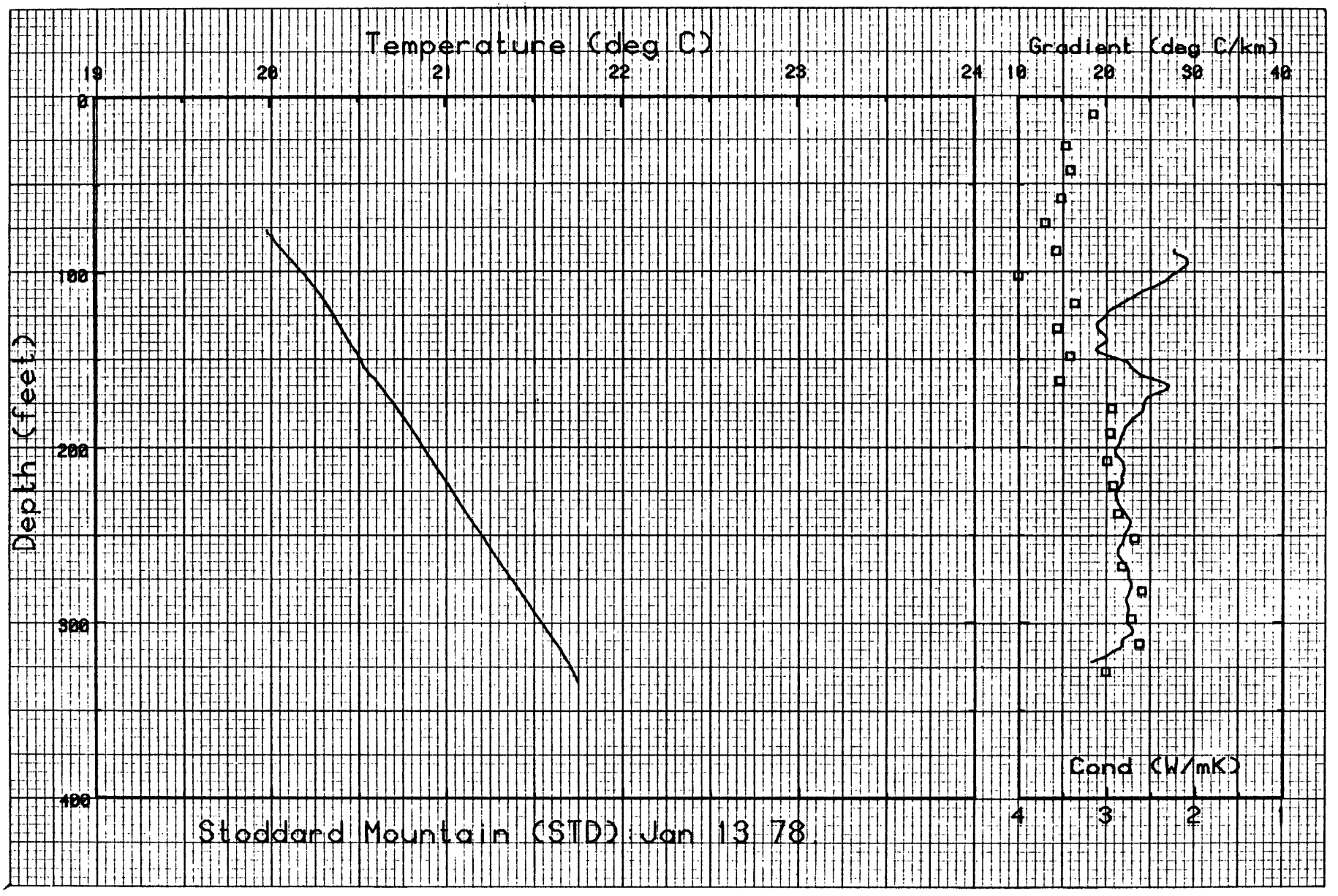

Figure 20. Temperature, gradient, and thermal conductivity profiles for STD.

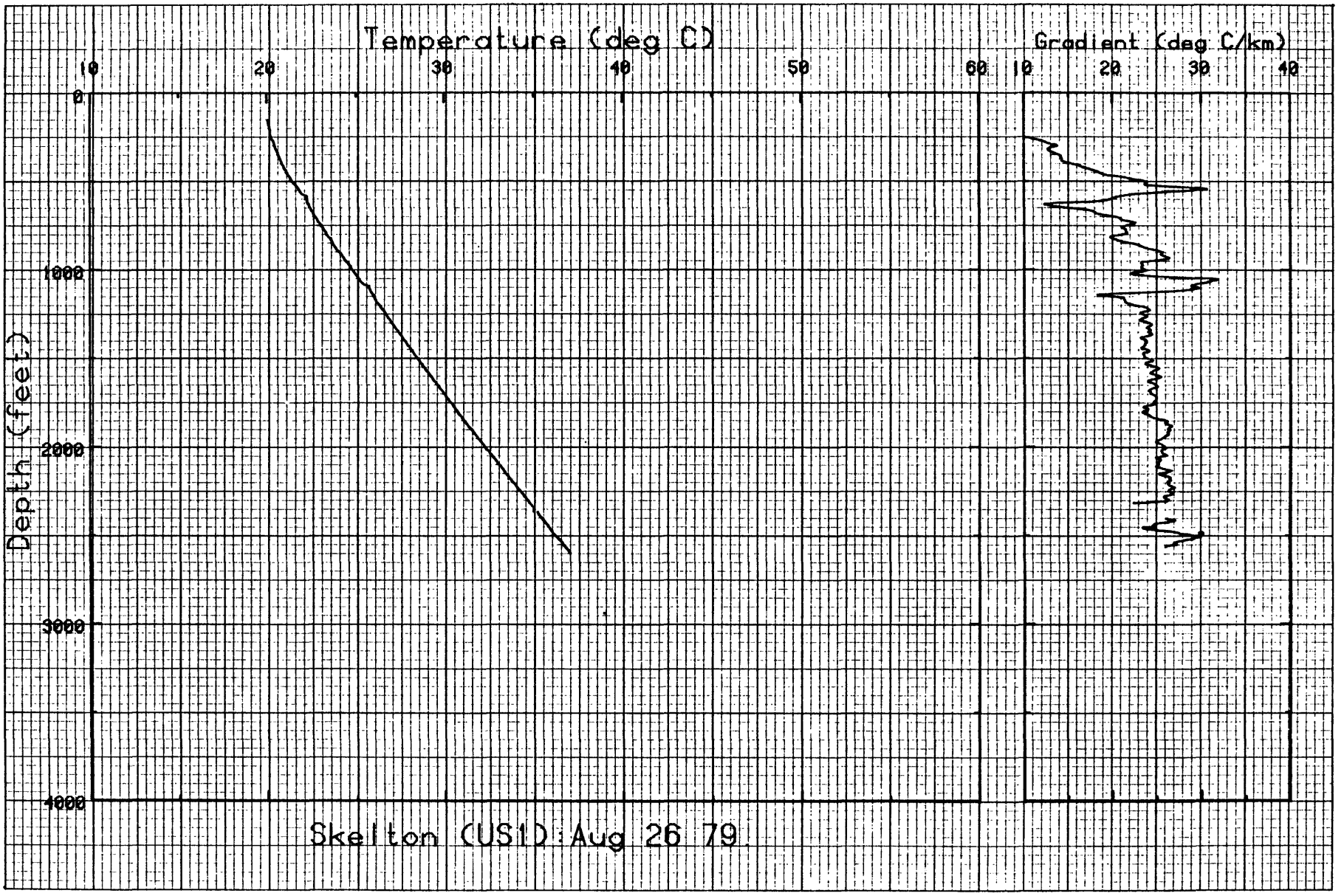

Figure 21. Temperature and gradient profiles for US1.

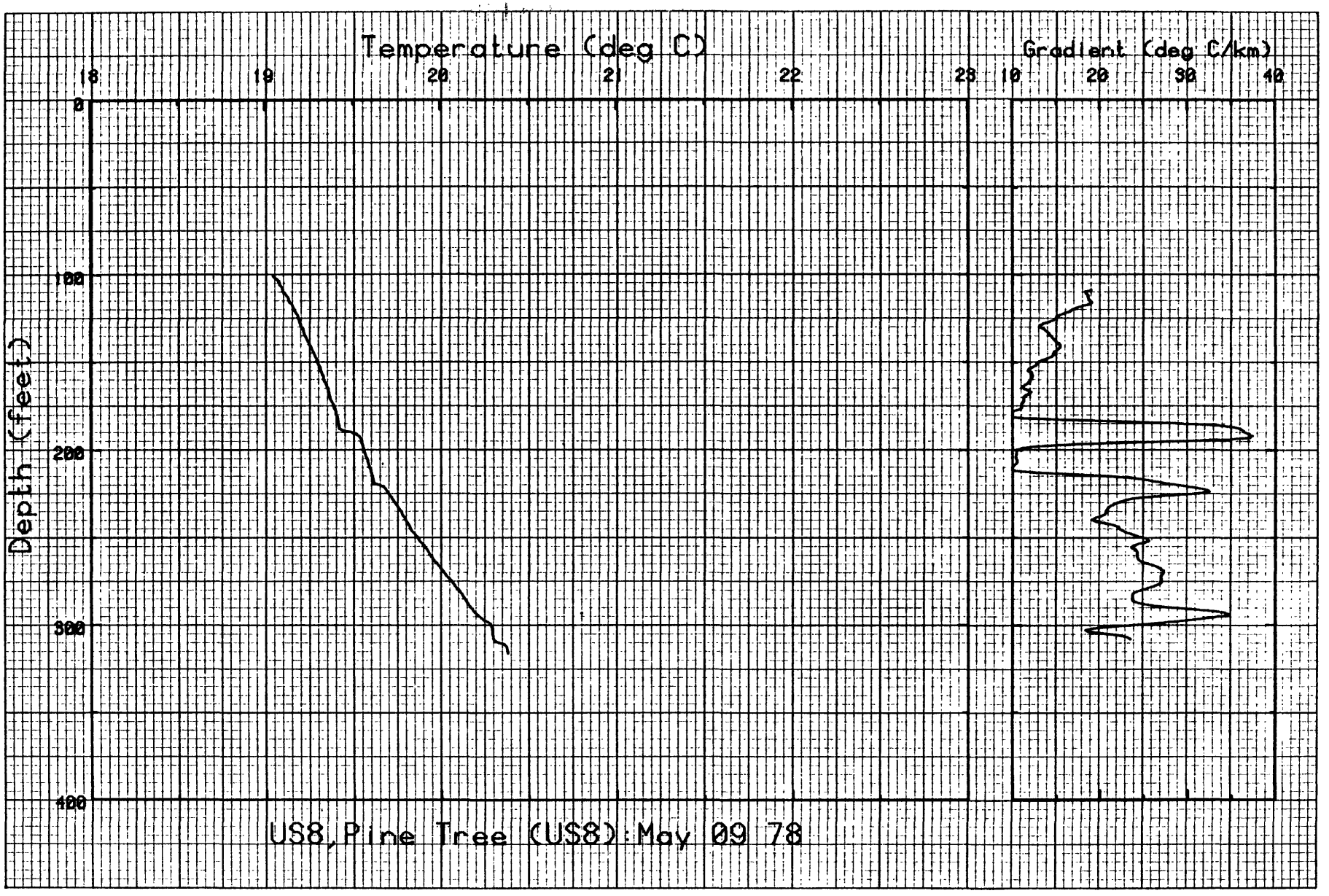

Figure 22. Temperature and gradient profiles for US8.

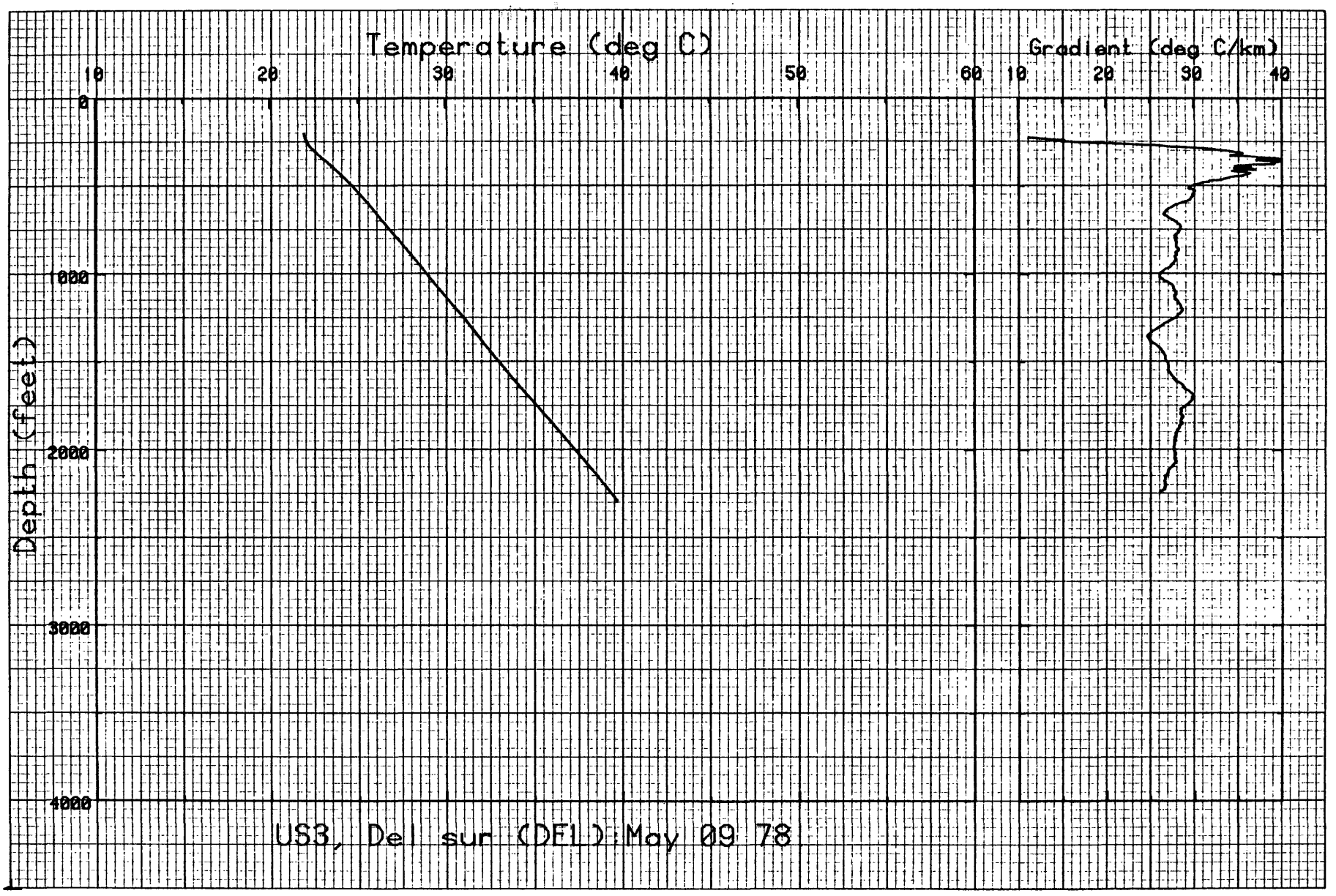

Figure 23. Temperature and gradient profiles for DEL.

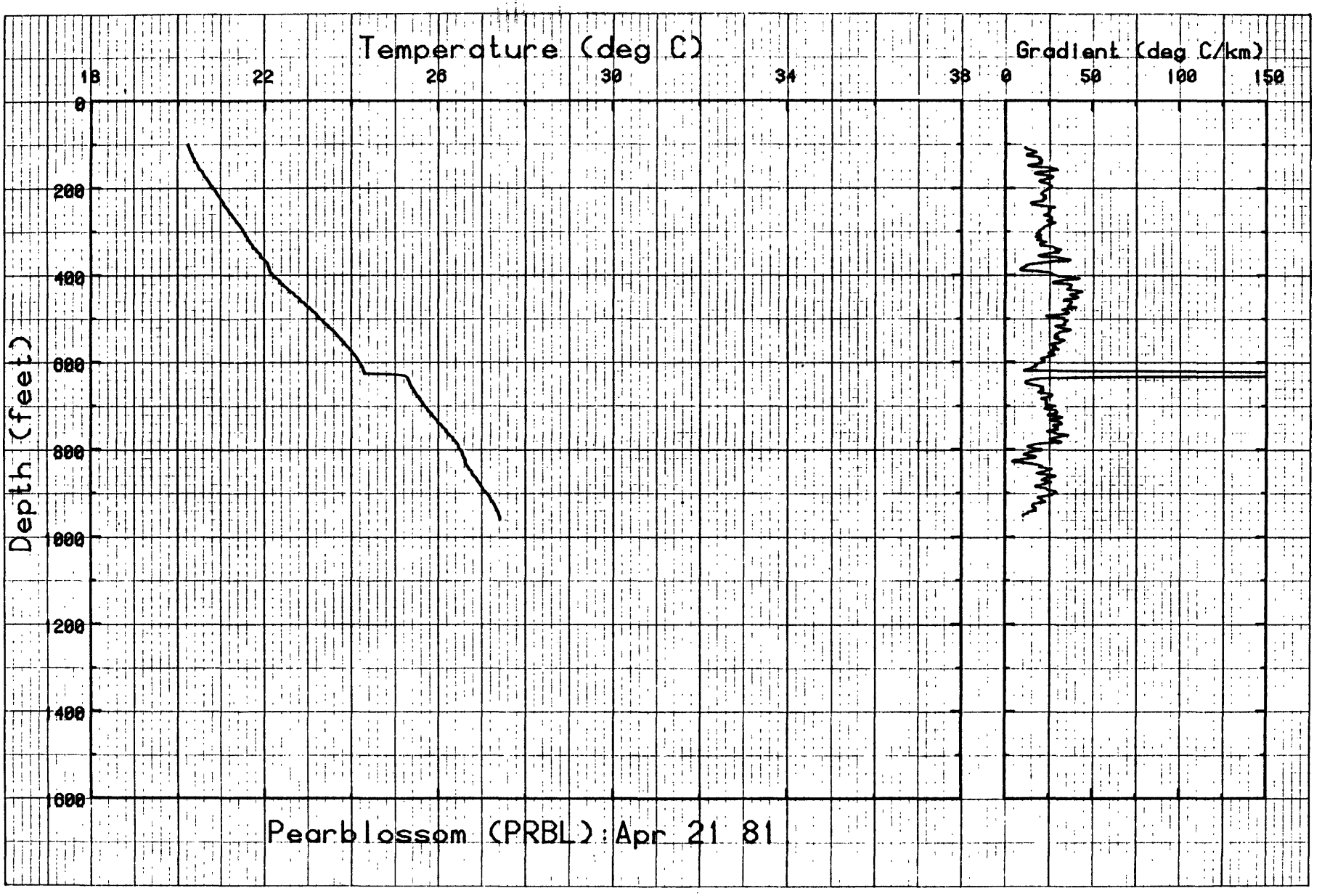

Figure 24. Temperature and gradient profiles for PRBL.

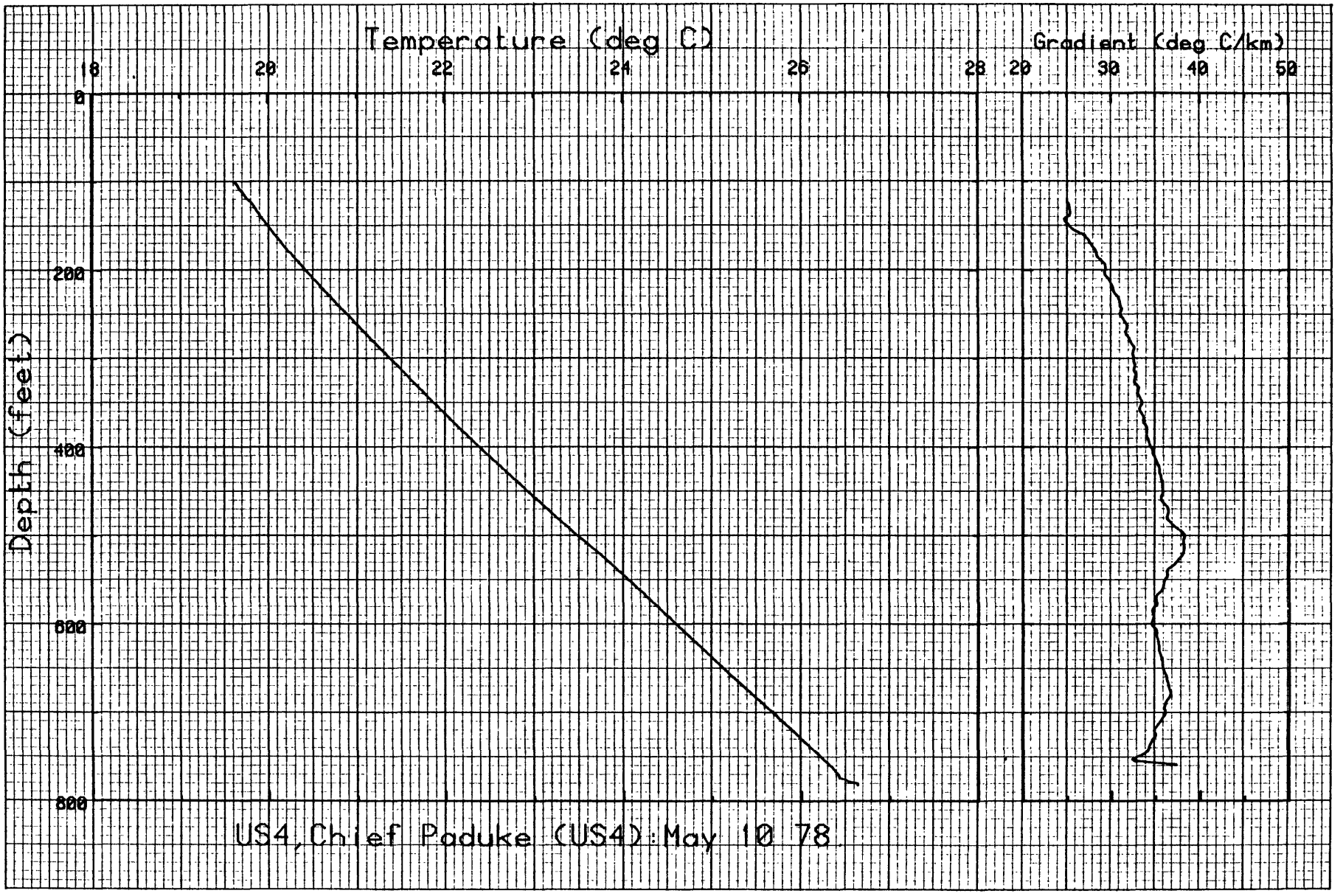

Figure 25. Temperature and gradient profiles for US4.

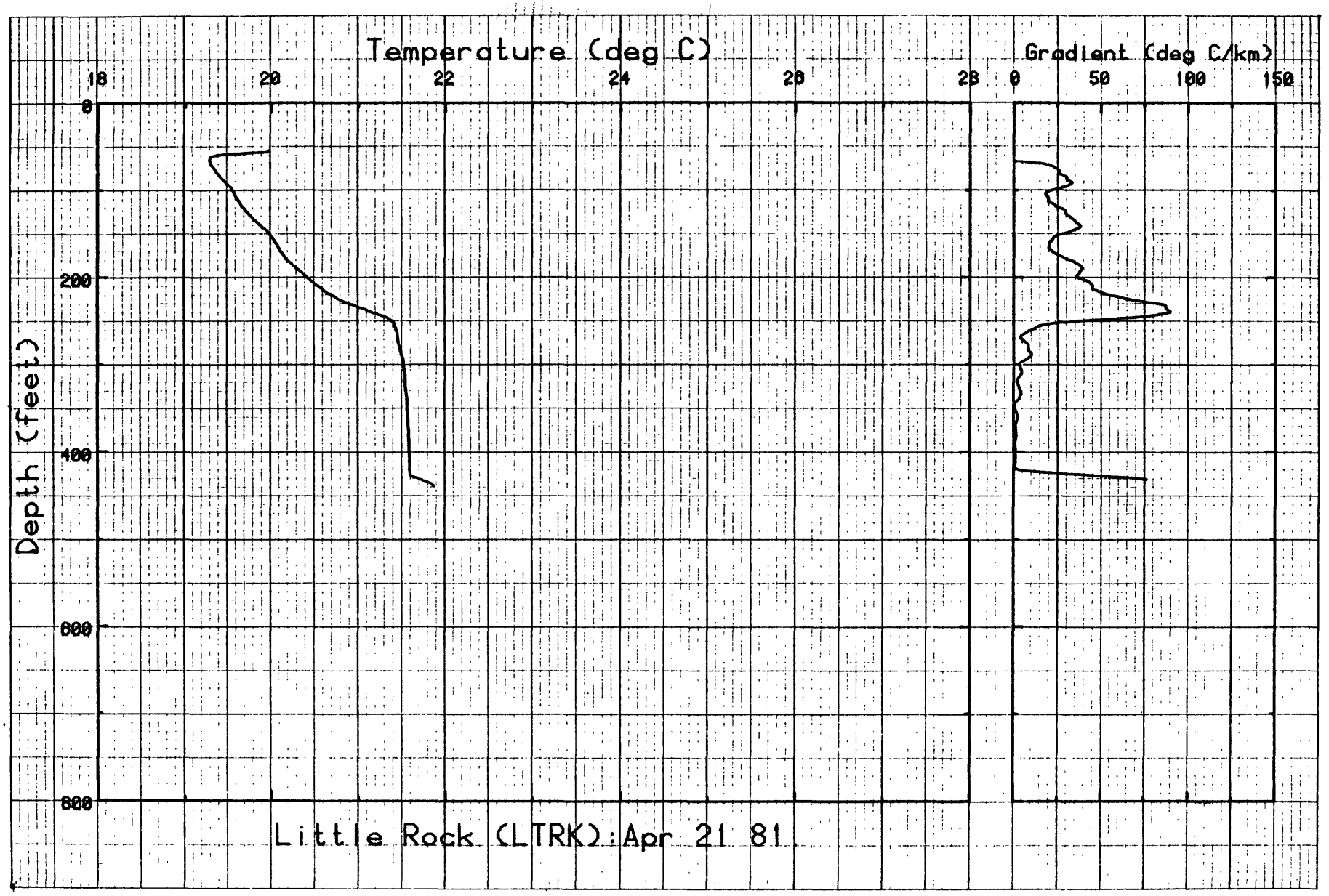

Figure 26. Temperature and gradient profiles for LTRK.

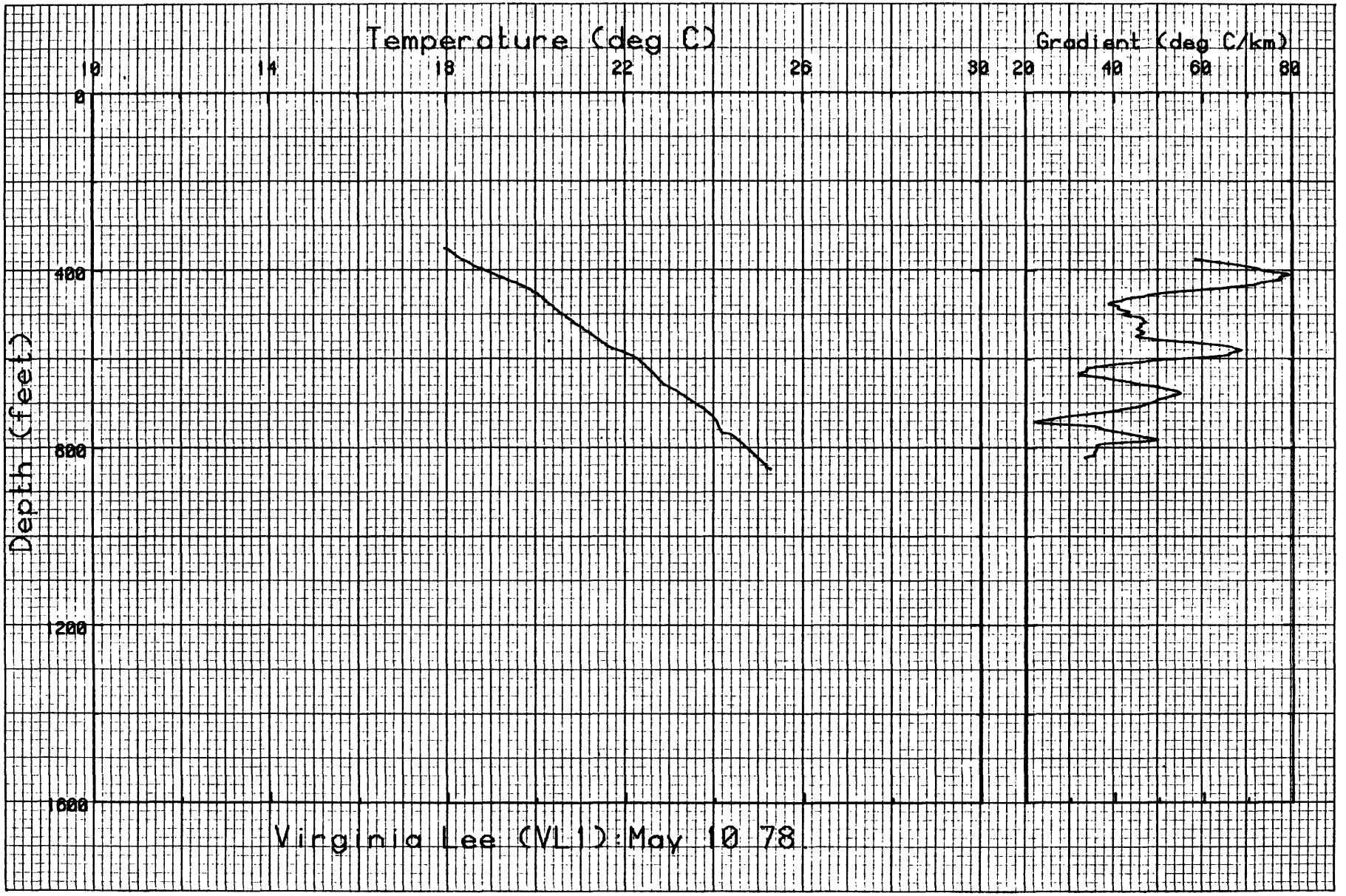

Figure 27. Temperature and gradient profiles for VL1.

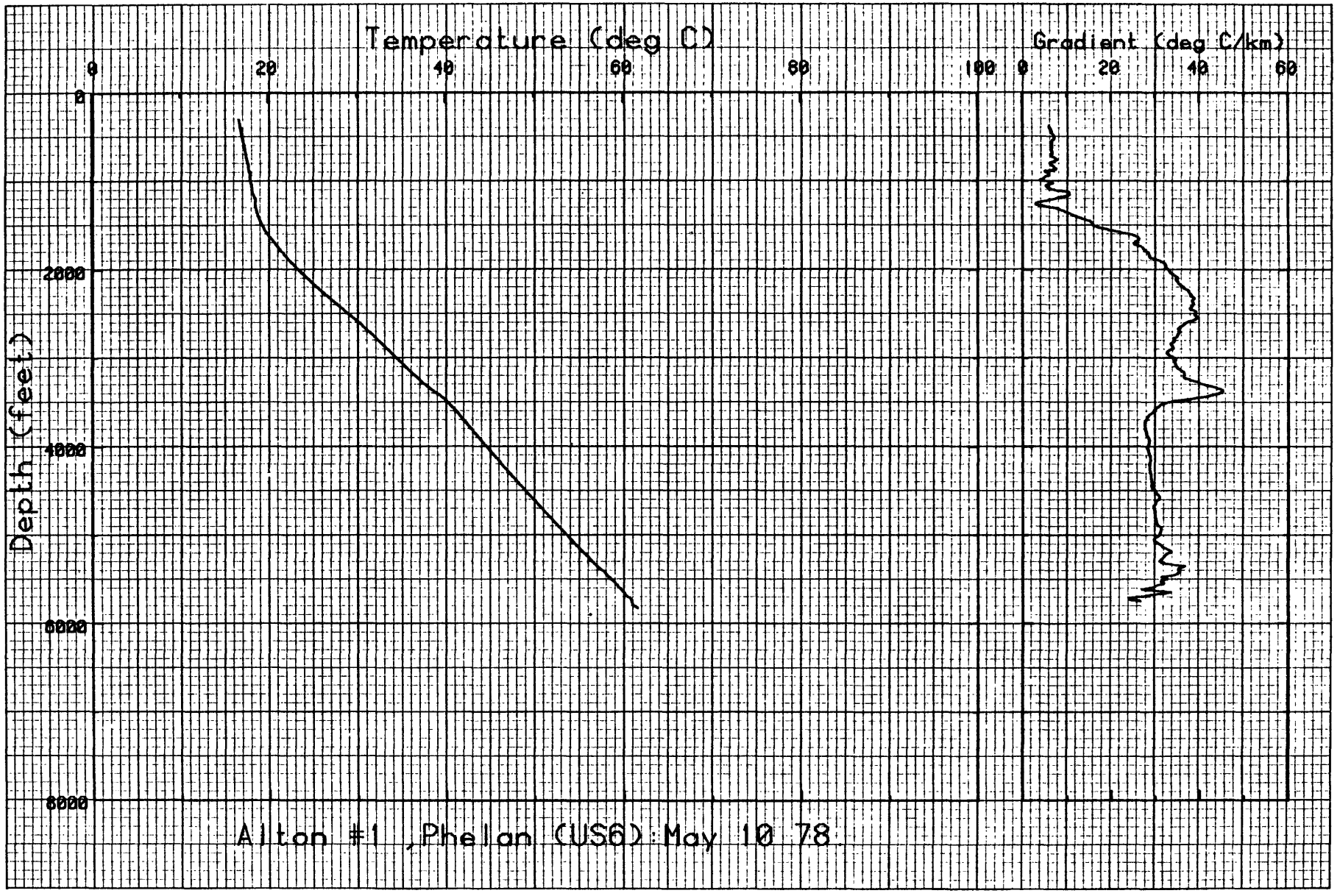

Figure 28. Temperature and gradient profiles for US6.

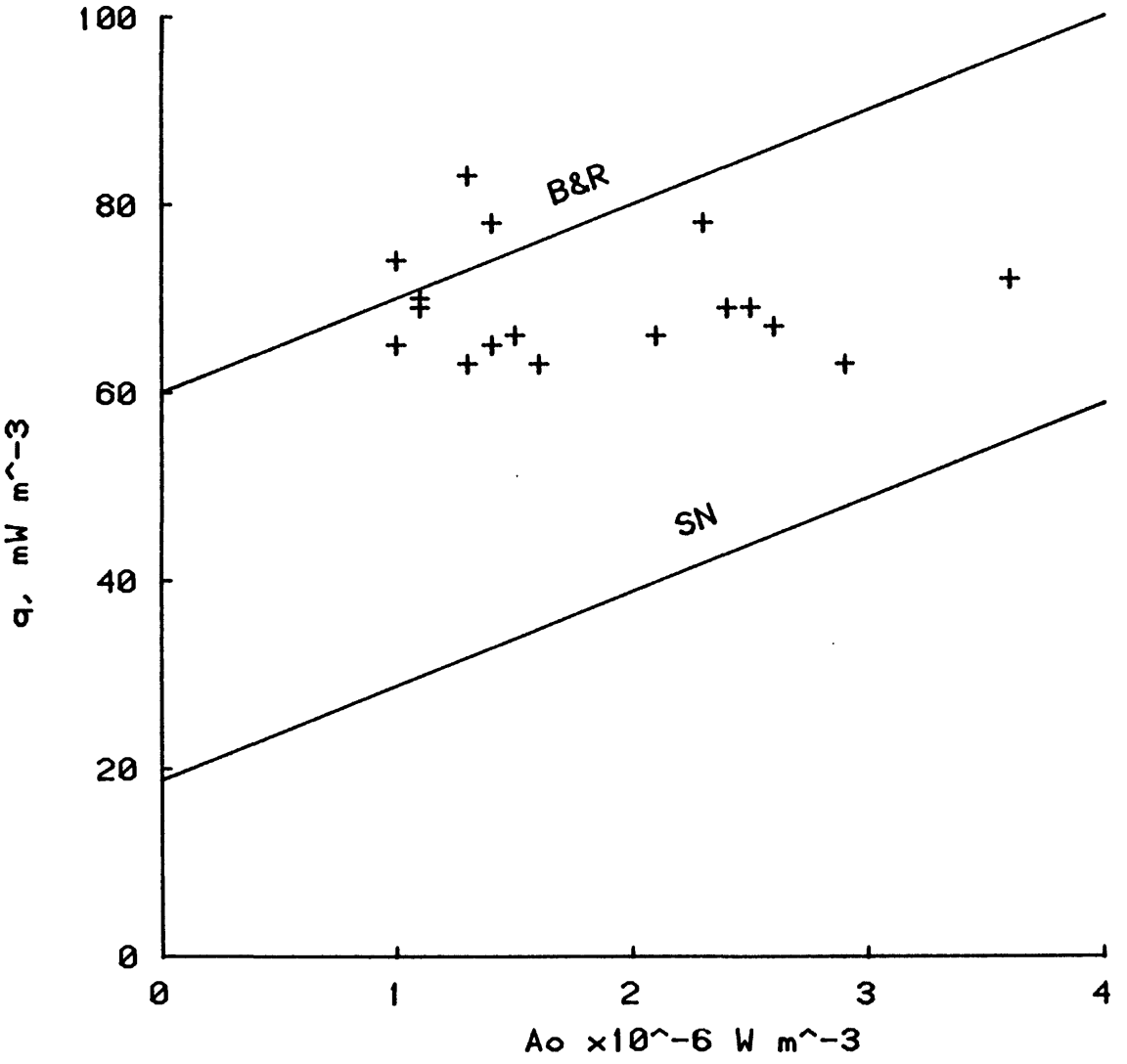

Figure 29. Heat flow (q) versus heat production (A_o) for the wells near Cajon Pass (CAJN). Lines are for the Basin and Range and for the Sierra Nevada (B&R and SN, Roy and others, 1968).

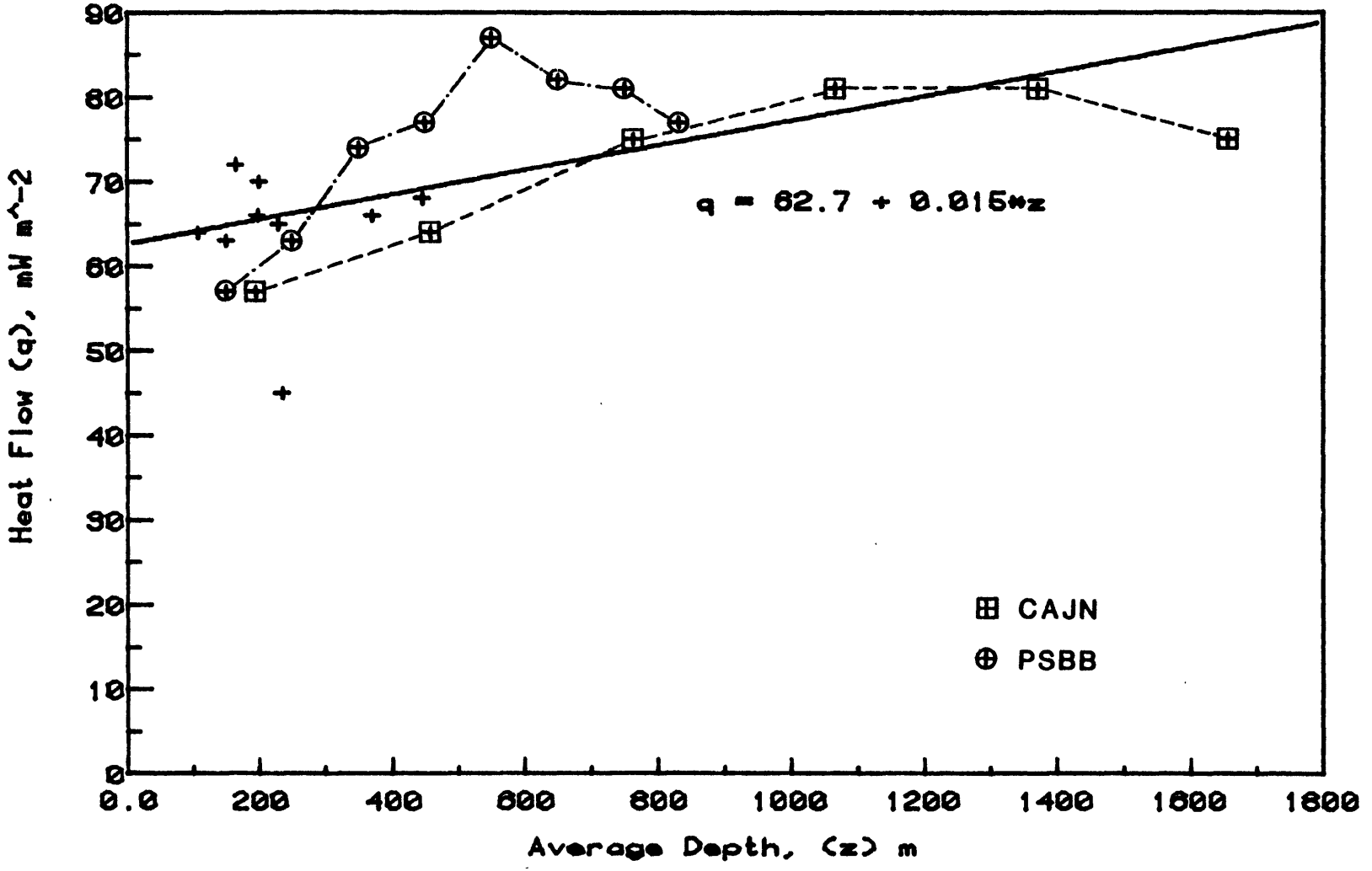

Figure 30. Heat flow versus average depth for sites in Figure 1 within 10 km of the San Andreas fault. Straight line is the formal least-squares fit.

TABLE 1. Heat flow in the vicinity of Cajon Pass (see Figure 1)

Well Designation	Depth range feet	Depth range m	Γ °C km^{-1} (SE)	N	$\langle K \rangle^{-1}$ (SE) W m^{-1} K^{-1}	q (SE) mWm^{-2}	q_{corr}***	A_o μWm^{-3}
LH1*	400- 690	120- 210	27.70 (0.09)	30	2.60 (0.02)	72 (1)	72	3.6
LH2*	600- 920	180- 280	22.21 (0.04)	25	2.62 (0.02)	58 (2)	65	1.4
LH3*	500- 800	150- 250	32.80 (0.14)	52	2.45 (0.04)	80 (2)	70	1.1
US7	400- 800	122- 244	24.74 (0.01)	6	2.49 (0.04)	62 (1)	57	
PSA	230- 750	71- 229	34.87 (0.02)	10	1.88 (0.05)	66 (1)	63	1.6
PSB	200- 500	61- 152	27.22 (0.01)	5	2.35 (0.12)	64 (3)	64	1.0
	500- 803	152- 245	29.80 (0.02)	6	2.23 (0.14)	66 (4)	66	
PSBB†	330-2830	100- 862					74	1.0
PSC	150- 700	46- 213	20.51 (0.01)	12	3.07 (0.14)	63 (2)	63	1.3
BBUT**	400-2110	122- 644				69 (1)	69	2.5
PSD	370- 640	115- 195	25.20 (0.05)	13	2.61 (0.08)	66 (2)	66	2.1
PSE	200- 740	91- 225	24.76 (0.03)	8	2.77 (0.09)	69 (2)	69	
HVI	213- 350	65- 107	22.10 (0.07)	9	3.02 (0.06)	67 (2)	67	2.6
HIVS	425- 575	130- 175	21.75 (0.05)	3	2.91 (0.02)	63 (1)		
	575- 900	175- 274	24.28 (0.18)	8	2.68 (0.04)	65 (1)	64	
	900-1840	274- 570	26.04 (0.01)	25	2.50 (0.03)	65 (1)		
PSF	200- 350	61- 107	24.45 (0.05)	11	2.81 (0.11)	69 (3)	69	2.4
CCT	200- 500	61- 152	26.12 (0.05)	8	2.64 (0.04)	69(1)	69	1.1
KJN	100- 330	30- 101	29.51 (0.05)	16	2.81 (0.05)	83 (2)	83	1.3
CAJN††	280-5867	85-1788				98 (3)	69	1.4
SB10*	1020-1440	311- 440	22.19 (0.06)	67	2.62 (0.04)	58 (1)	66	1.5
SB2*	1410-1515	430- 462	24.56 (0.14)	26	2.55 (0.06)	63 (2)	68	
SB5*	660- 885	200- 270	17.66 (0.26)	16	2.49 (0.07)	44 (2)	45	
GMC	200- 500	61- 152	23.41 (0.02)	20	3.29 (0.10)	77 (2)	78	2.3
STD	160- 315	49- 96	22.07 (0.02)	11	2.86 (0.07)	63 (2)	63	2.9

‡From Table 2, p. 7932 of Henyey and Wasserburg (1971).
†For details, see Table 2.
‡‡For details, see Table 3.
††For details, see Table 4.
***Corrected for steady-state topography, except for CAJN (see Table 4).

TABLE 2. Heat flow over 100 m intervals in PSBB

Depth range m		Mean temp. °C	Γ °C/km	(SE)	N	<K>, W m^{-1} K^{-1} Obs	(SE)	Corr*	q (mWm^{-2}) Obs	(SE)	Corr*
100	200	21	22.94	(0.06)	7	2.49	(0.05)	2.50	57	1	57
200	300	23	25.49	(0.04)	8	2.45	(0.05)	2.46	62	1	63
300	400	26	29.52	(0.02)	8	2.49	(0.05)	2.49	74	2	74
400	500	29	30.73	(0.02)	12	2.50	(0.04)	2.50	77	1	77
500	600	32	33.97	(0.05)	8	2.59	(0.03)	2.57	88	1	87
600	700	35	32.05	(0.04)	8	.2.58	(0.05)	2.55	83	2	82
700	800	38	33.25	(0.04)	8	2.47	(0.05)	2.44	82	2	81
800	862	41	31.54	(0.05)	6	2.47	(0.07)	2.43	78	2	77
								Average	75	2	74

*Corrected for the in situ variation of conductivity with temperature.

TABLE 3. Heat flow as a function of depth at Black Butte (BBUT)

Depth range m	Γ, °C/km	N	$\langle K \rangle$ W m^{-1} K^{-1}	q mWm^{-2}
122-244	23.33±0.02	11	2.86±0.06	67±1
244-366	24.25±0.01	10	2.94±0.03	71±1
366-488	24.41±0.01	10	2.89±0.03	70±1
488-644	24.32±0.01	13	2.79±0.08	68±2

TABLE 4. Heat flow as a function of depth at Cajon Pass

Depth range m	Γ, °C/km	Terrain corr.	Uplift corr.	Erosion corr.	Γ, °C/km corr.	N	<K> W m^{-1} K^{-1}	q	q_{corr} mWm^{-2}
85-305	37.02±0.05	-5.7	+3	-8.4	25.9	8*	2.64±0.12 2.2±0.2	98	68 57
305-610	36.65±0.05	-4.8	+3	-8.2	26.6	10*	2.83±0.08 2.4±.2	104	75 64
610-914	34.73±0.08	-4.0	+3	-7.8	25.9	10	2.90±0.09	101	75
914-1219	35.53±0.1	-3.3	+3	-7.2	28.0	10	2.89±0.15	103	81
1219-1524	37.10±0.05	-2.8	+3	-6.9	30.4	10	2.68±0.10	99	81
1524-1788	35.1±0.1	-2.4	+3	-6.6	29.1	10	2.57±0.04	90	75

*Upper, assuming zero porosity; lower assuming a porosity of 11.2±5%.

TABLE 5. Thermal conductivity, density, and porosity of outcrop samples from the Punchbowl (TP) and Crowder (TC) Formations, Cajon Pass, California

Sample	Thermal conductivity $W\ m^{-1}\ K^{-1}$	Unsaturated density $g\ cm^{-3}$	Porosity %
Tc 1a	2.16	2.09	20.9
Tc 1b	2.20	2.26	12.5
Tc 2	1.74	2.18	16.8
Tc 3	1.90	2.53	5.7
Tp 2a	2.50	2.28	11.7
Tp 3	2.12	2.34	11.4
Tp 5a	2.68	2.42	7.5
Tp 5b	2.81	2.41	7.7
Tp 6	2.90	2.47	6.4

TABLE 6. Temperature gradients, inferred lithology, and heat-flow estimates for wells for which no samples are available (see Figure 1)

Well	Depth range ft	Depth range m	Γ, °C/km	Lithology	K range $W\ m^{-1}\ K^{-1}$	q range mWm^{-2}
US1	1200-2600	366- 793	25	Granite?	2.5-3.3	62-82
US8	220- 300	67- 91	22.5	Alluvium	1.0-1.5	22-33
DEL	500-2275	152- 693	27.5	Fanglomerate	1.7-2.5	47-69
PRBL	400- 960	122- 293	31	Andesite?	1.7-2.5	53-78
US4	500- 760	152- 232	37	Shale, sdst	1.5-2.0	56-74
LTRK	70- 430	21- 131	21.5*	Granite	2.5-3.3	54-71
VL1	450- 850	137- 259	42	Shale, sdst	1.5-2.0	63-84
US6	3500-5800	1067-1768	30	Fanglomerate	1.7-2.5	51-75

*Large hydrologic disturbance, see Figure 26.